

ARTICLE OPEN



APOE deficiency inhibits amyloid-facilitated (A) tau pathology (T) and neurodegeneration (N), halting progressive ATN pathology in a preclinical model

Sarah Vanherle^{1,6}, Art Janssen^{1,6}, Manuel Gutiérrez de Ravé^{1,6}, Bieke Janssen¹, Chritica Lodder¹, Pablo Botella Lucena¹, Sofie Kessels¹, Jana Hardy¹, Eline Vandeput¹, Yanyan Wang¹, Ilie-Cosmin Stancu¹, Andrei Segal^{2,3}, Markus Kleinewietfeld^{4,5}, Thomas Voets^{2,3}, Bert Brône¹, Suresh Poovathingal³, Yeranddy A. Alpizar^{1,2,3} and Ilse Dewachter¹✉

© The Author(s) 2025

In AD, amyloid pathology (A) precedes progressive development of tau pathology (T) and neurodegeneration (N), with the latter (T/N) processes associated with symptom progression. Recent anti-amyloid beta (A β) clinical trials raise hope but indicate the need for multi-targeted therapies, to effectively halt clinical AD and ATN pathology progression. *APOE*-related putative protective mutations (including *APOE3*Christchurch, *RELN-COLBOS*) were recently identified in case reports with exceptionally high resilience to autosomal dominant AD. In these cases, Nature provided proof of concept for halting autosomal dominant AD and ATN progression in humans, despite a high amyloid load, and pointing to the *APOE* pathway as a potential target. This is further supported by the recent identification of *APOE4* homozygosity as genetic AD. Here we studied the role of *APOE* in a preclinical model that robustly mimics amyloid-facilitated (A) tau pathology (T) and subsequent neurodegeneration (N), denoted as ATN model, generated by crossing 5xFAD (F^{+}) and TauP301S (T^{+}) mice. We show that *APOE* deficiency, markedly inhibited progression to tau pathology and tau-induced neurodegeneration in this ATN model, despite a high A β load, reminiscent of the high resilience ADAD case reports. Further study identified, despite increased A β load (W02 stained), a significant decrease in compacted, dense core plaques stained by ThioS in *APOE* deficient ATN mice. Furthermore, single-cell RNA sequencing (scRNA-seq) showed a crucial role of *APOE* in microglial conversion beyond homeostatic microglia to reactive and disease associated microglia (DAM) in this ATN preclinical model. Microglial elimination significantly decreased amyloid-driven tau pathology, in the presence of *APOE*, but not in *APOE* deficient mice. Together the data demonstrate that *APOE* deficiency inhibits amyloid-driven tau pathology and subsequent neurodegeneration, by pleiotropic effects including prevention of dense core plaque formation and halting conversion of homeostatic microglia. We here present a model recapitulating inhibition of amyloid-facilitated tau pathology by *APOE* deficiency despite high A β load, important for understanding the role of *APOE*, and *APOE*-dependent processes in ATN progression and its therapeutic exploitation in AD.

Molecular Psychiatry; <https://doi.org/10.1038/s41380-025-03036-7>

INTRODUCTION

Alzheimer's disease (AD) presents a major medical and socio-economic challenge to patients, their entourage, and society [1]. After over 100 years of intensive research and disappointing clinical trial results, recent anti-A β clinical trials finally yielded significant positive results [2–4], raising hopes for advances in AD therapy [2–6]. Nevertheless, the clinical impact of these innovative treatments remains limited, highlighting the need to better understand the mechanistic link between A β pathology and downstream pathologies to develop therapies that effectively halt AD progression [2–7]. AD brains are characterized by progressive development of A β pathology (A), tau pathology (T), and neurodegeneration (N), denoted as ATN pathology [8–14].

Amyloid pathology progresses spatiotemporally by Thal stages, preceding by up to a decade, the spread of tau pathology by Braak stages [8–15], closely associated with progressive neurodegeneration and symptoms [8–18]. This characteristic ATN progression presents the biological definition of AD, summarized as the ATN-framework [8–16]. Importantly, early onset autosomal dominant AD (ADAD) mutations –leading to altered A β biogenesis and A β pathology–, invariably cause progressive tau pathology and neurodegeneration, thereby indicating a causal link between these processes [19–21] and an interesting therapeutic window. The underlying molecular and cellular mechanisms of progression beyond amyloid pathology, as well as the toxic A β and tau culprits [22–27], remain to be unequivocally defined, which is required to

¹Department of Neurosciences, Biomedical Research Institute BIOMED, Hasselt University, Hasselt, Belgium. ²Laboratory of Ion Channel Research, Department of Cellular and Molecular Medicine, KU Leuven, Leuven, Belgium. ³VIB Center for Brain & Disease Research, Leuven, Belgium. ⁴VIB Laboratory of Translational Immunomodulation, Center for Inflammation Research (IRC), Hasselt University, Diepenbeek, Belgium. ⁵Department of Immunology and Infection, Biomedical Research Institute (BIOMED), Hasselt University, Diepenbeek, Belgium. ⁶These authors contributed equally: Sarah Vanherle, Art Janssen, Manuel Gutiérrez de Ravé. ✉email: ilse.dewachter@uhasselt.be

Received: 3 July 2024 Revised: 12 March 2025 Accepted: 15 April 2025

Published online: 30 April 2025

design therapeutic strategies that halt ATN progression and effectively impact AD symptom progression.

In this respect, the recent discoveries of putative protective mutations in Apolipoprotein E3 (*APOE3*) are milestone findings towards strategies to slow or halt AD progression [28]. A putative protective homozygous *APOE3*Christchurch mutation (*APOE3Chch* - R136S - receptor binding domain) was identified in an *ADAD PS1* mutation carrier with high amyloid load but limited tau pathology and neurodegeneration, and 30 years delayed symptom onset [29, 30]. *APOE3Chch* mutation, associated with loss of function aspects of APOE-receptor and HSPG binding, and loss of APOE-A β -interaction [29, 30], may halt early amyloid-induced tau seeding, and may constitute a compelling approach to slow ATN progression [31]. Along this line, other putative protective effects have been associated with *APOE3 Jacksonville* variants in sporadic cases [28]. In a similar vein, another case report of an *ADAD PS1* mutation carrier with high amyloid load but decreased tau pathology and neurodegeneration exhibited exceptionally high resilience with delayed symptom onset until 67 years of age [32, 33]. This individual harbored a *RELN-COLBOS* mutation with increased APOE-receptor binding by Reelin-COLBOS, including APOER2 and VLDL-receptors [32], and was possibly protective against ATN progression [32, 33], further supporting the APOE pathway as a potential approach for modifying AD progression. This is aligned with knowledge of *APOE* as a major genetic late onset AD risk factor [34–36], with *APOE2* lowering and *APOE4* raising AD risk [34, 37]. And most recently, *APOE4* homozygosity was identified as a distinct genetic AD form [38]. Therefore, Nature itself provided with these high resilience *ADAD* cases a ‘proof of concept’ for effectively modifying or halting AD and ATN progression despite high amyloid load, pointing to APOE and its pathway as potential targets. However, further detailed study and mechanistic understanding is needed to therapeutically exploit this ‘proof of concept’.

Preclinical models have helped shed insight into the ability of APOE and/or human APOE isoforms to modulate amyloid and tau pathology independently. APOE modulates amyloid pathology in amyloid only models by altering amyloid plaque seeding [28, 39], plaque compaction, and microglial association with plaques [32, 37, 39–44]. However, whether these APOE-dependent changes in A β pathology effectively impact or can halt progression to downstream ATN processes remains to be determined. This is a non-trivial question considering the need for targets that can effectively halt A β -facilitated tau pathology and neurodegeneration, associated with symptom progression. Human APOE isoforms modulate tau pathology (*APOE4* > *APOE3* [40]) in a tauopathy only model, i.e. in TauP301S transgenic mouse model [40]. Human APOE isoforms also influence early tau-seeding, in dystrophic neurites near amyloid plaques in an amyloid APPS1 transgenic mouse with injected PHF tau [45], but lacking robust amyloid induced NFT pathology and associated neurodegeneration linked to symptom progression. The latter was also shown for the *APOE Christchurch* mutation [31, 46] in an early tau-seeding model on dystrophic neurites near amyloid plaques. Assessing the role of APOE in ATN progression requires preclinical models that recapitulate robust neurodegeneration (N) closely associated with amyloid (A)-facilitated and -accelerated tau pathology (T) (including mature NFTs), thereby recapitulating full-blown and progressive ATN pathologies. To this end, *F⁺T⁺* mice, generated by crossing 5xFAD to TauP301S mice, display robust amyloid-facilitated tau pathology and associated neurodegeneration, and constitute a robust model for mechanistic analysis of the link between these pathologies and ATN progression [47–52].

Besides the characteristic progressive ATN pathology, AD brains display a strong inflammatory component, encompassing microgliosis, as an important hallmark of AD. Notably, besides modulating ATN via direct effects on A β and/or tau pathologies, or potentially their receptor binding [53–55], APOE is also crucial

to determine microglial phenotypes and their associated functions [56–58]. Microglial activation -and APOE- are increasingly considered active contributors to AD pathology and ATN progression [7, 59–65]. AD brains invariably present with microgliosis, associated with amyloid and tau pathology [9, 66–71]. Microglia modulate both amyloid and tau pathology, in models mimicking these pathologies independently [47, 72–75]. During neurodegeneration, microglia adopt a range of transcriptomic profiles, following a trajectory from homeostatic, to reactive and DAM states [47, 56, 57, 76, 77]. Many genes expressed or upregulated in microglia, beyond *APOE*, are AD risk factors [78, 79], pointing to their crucial role in the disease process. Thus, although microglia clearly contribute to the pathogenetic process in AD, whether these effects are detrimental or protective is context dependent, based on distinct microglial populations, disease stage, and associated ATN pathologies. However, to therapeutically target microglia requires detailed understanding of their phenotypes and respective contributions in the presence of progressive development of combined ATN pathologies.

Here, we analyzed the inhibitory potential of APOE deficiency in ATN progression, i.e., amyloid-facilitated tau pathology, with subsequent neurodegeneration, to shed insight into the potential and mechanisms of APOE-mediated slowing of ATN progression. We leveraged the *F⁺T⁺* model, which recapitulates robust ATN pathology, generated by crossing 5xFAD and TauP301S transgenic mice [47–50]. We here show that APOE deficiency inhibited amyloid-facilitated tau pathology and associated neurodegeneration reflected in hippocampal atrophy, reminiscent of delayed ATN pathology linked to *APOE3Chch*. We furthermore show that APOE deficiency increased A β load but decreased dense core plaque formation. Also, APOE deficiency blocked the conversion of homeostatic microglia to reactive and DAM microglia. And eliminating microglia significantly decreased amyloid-driven tau pathology, in the presence of APOE but not in APOE deficient mice. Taken together, we demonstrate a role for APOE deficiency in amyloid-facilitated tau pathology and subsequent neurodegeneration through multifactorial pathways, including preventing dense core amyloid pathology and inhibiting conversion of homeostatic microglia. The presented findings are crucial for a better understanding of the executive role of APOE on ATN progression and may open new avenues for future AD therapy development.

METHODS

Animals

The in house well-characterized strain of hemizygous 5xFAD mice, overexpressing mutant human APP695, (3 EOFAD mutations: K670N/M671L (Sw), I716V (Fl), V717I (Lo)) and mutant human PS1 (2 EOFAD mutations: (M146L and L286V)) driven by the Thyl promoter, generated by the group of R. Vassar [48], was crossed with the hemizygous TauP301S transgenic mice (PS19) [50], expressing human Tau-P301S (1N4R) driven by the mouse PrP promoter, to obtain the *F⁺T⁺* strain. These strains are well-characterized in the research group [47, 49, 73, 80–83]. The parental (single) 5xFAD mice develop amyloid plaques at around 3 months of age. The parental (single) hemizygous TauP301S transgenic mice (PS19; *T⁺* mice) develop tau pathology at around 11 months, associated with progressive development of a neurodegenerative phenotype, including motor deficits, clasping, hunchback and premature death. Tau pathology, specifically somatodendritic AT8 staining and NFTs are not detected at 6 months of age. Both parental lines display a consistent development of pathological changes in our hands [47, 49, 73, 80–83]. The phenotype of TauP301S mice appears later than initially described by Yoshiyama and colleagues [50], due to a well-described genetic drift of the parental strain, while also the use of hemizygous mice, potential effects of sub-strain generation by breeding, and housing conditions may contribute to this effect. This genetic drift and less severe phenotype is well recognized and has been previously described, while the phenotype of the strain is conserved and is highly consistent and reproducible, reflected in studies by many groups [49, 84, 85]. The *F⁺T⁺* strain was generated by crossing the parental strains and showed an accelerated and aggravated tau-related

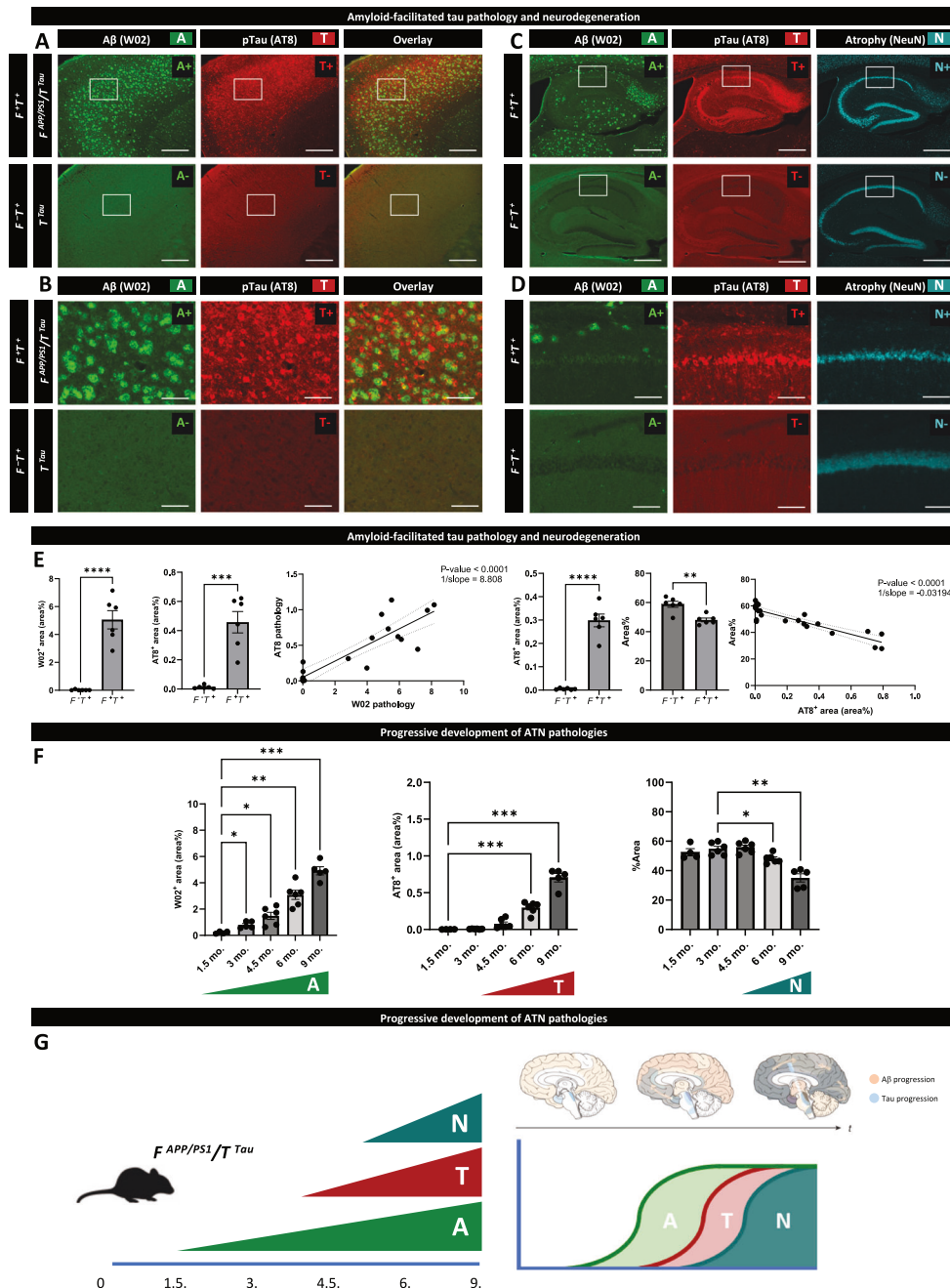


Fig. 1 $F^{+}T^{+}$ mice exhibited amyloid-facilitated tau pathology and neurodegeneration, or progressive ATN pathologies. **A** Representative images of the frontal cortex of $F^{+}T^{+}$ and $F^{-}T^{+}$ mice stained with W02 and AT8 antibody, respectively staining A β (first column) and p-tau pathology (second column), and overlay (third column), showing robust AT8 staining, in the presence of but not in the absence of amyloid pathology in $F^{+}T^{+}$ mice compared to $F^{-}T^{+}$ mice at 6 months of age. Scalebar represents 500 μ m. A detailed timeline of the appearance of ATN pathologies is presented in Fig. S1. **B** Higher magnifications of A β (first column), p-tau pathology (second column) and overlays (third column) are presented. Scalebar represents 125 μ m. **C** Representative images of the hippocampus of $F^{+}T^{+}$ and $F^{-}T^{+}$ mice stained with W02, AT8 and NeuN, respectively staining A β (first column, "A"), p-tau pathology (second column, "T") and neurons (third column, "N"), showing robust AT8 staining and hippocampal atrophy, in the presence of but not in the absence of amyloid pathology (respectively in $F^{+}T^{+}$ mice compared to $F^{-}T^{+}$ mice) at 6 months of age. Scalebar represents 500 μ m. **D** Higher magnifications of A β (first column), p-tau pathology (second column) and neurons (third column). Scalebar represents 125 μ m. **E** (Left panel) Quantitative analysis of W02 and AT8 stained area in the frontal cortex and their linear regression analysis ($p < 0.0001$, $1/\text{slope} = 8.808$), showing significant correlation. (Right panel) Quantitative analysis of AT8 stained area in the hippocampus and hippocampal area of $F^{+}T^{+}$ ($n = 6$) and $F^{-}T^{+}$ ($n = 6$) mice and their linear regression analysis ($p < 0.0001$, $1/\text{slope} = -0.03194$), showing significant negative correlation. Following normality testing unpaired student t-test was used. Results were presented as mean \pm standard error (SEM). $**p < 0.01$, $***p < 0.001$, $****p < 0.0001$. **F** Quantitative analysis of W02 and AT8 stained area and hippocampal area in $F^{+}T^{+}$ mice at different ages (1.5 mo. ($n = 4$), 3 mo. ($n = 6$), 4.5 mo. ($n = 6$), 6 mo. ($n = 6$) and 9 mo. ($n = 5$)). Following normality testing ANOVA tests were used. Results were presented as mean \pm standard error (SEM). $*p < 0.05$, $**p < 0.01$, $***p < 0.001$. **G** Schematic overview of the ATN mouse model over time (left) and the human ATN framework (the upper panel adapted from Jucker and Walker [121] (right)). A timeline with a detailed analysis of the appearance of the respective ATN pathologies in this ATN model is presented in Fig. S1.

phenotype (Fig. 1, Fig. S1). The F^{+T+} strain was further crossed with APOE deficient mice on a C57BL/6J background to generate the full F^{+T+} ApoE KO mouse line. In this work, no behavioral analysis was conducted on the animals in order to focus on changes of pathological A β and tau, previously found to strongly correlate with behavioral and functional deficits associated with progressive pathology in the respective brain regions [22, 24, 25, 86–88]. Animals were housed under regular conditions in a temperature-controlled room around 23 °C on a 12 h day-night light cycle with *ad libitum* access to food and water. Sample size calculations were performed using G*Power based on related analyses in previous publications [47, 49]. The ethical committee for animal welfare of Hasselt University approved all the performed experiments.

Mice treatment

PLX3397 (Adooq Bioscience, Irvine, CA, USA), a well characterized Colony stimulated factor 1 receptor (CSF1R) inhibitor, was used to eliminate microglia. PLX3397 was mixed in a concentration of 1 g PLX3397 per kg normal chow (V1524-000, Ssniff) and mice were randomly and blinded to the researcher allocated to a group and treated from 3 months onwards until the age of 6 months. The protocol for optimal microglial elimination using this treatment was previously optimized and performed accordingly [47].

Immunohistological analysis

Immunohistological analysis was performed according to well-established protocols in the research group [47, 49, 73, 80–83]. Briefly, mice brains were dissected after 2 min transcardiac perfusion (PBS, 4 °C) and fixed in 4% paraformaldehyde-PBS (4 °C). Stainings were performed on free-floating sagittal sections (40 μ m), using anti-phospho-tau (Ser202, Thr205) monoclonal antibody (AT8; MN1020; Thermo Fisher Scientific, Waltham, MA, USA), anti-A β (W02; MABN10; Merck Millipore, Burlington, MA, USA) anti-Iba1 (019-19741; Fujifilm Wako, Neuss, Germany), anti-neuronal nuclei (NeuN; ABN78; Merck Millipore, Burlington, MA, USA), anti-CD68 (MCA1957; Bio-Rad, Hercules, CA, USA), anti-TSPO (EPR5384; Abcam, Cambridge, UK), anti-LAMP1 (sc-20011; Santa Cruz Biotechnology, Dallas, TX, USA) and anti-GSK3 β (610201; BD Transduction Laboratories, USA) antibodies, followed by incubation with the appropriate Alexa Fluor-488, -568 or -647 coupled secondary antibodies. ThioFlavin S, Gallyas silver and pFTAA stainings were performed as described previously, using a standardized protocol [8, 85]. Images were acquired with a Leica DM400 B LED fluorescence microscope (Leica, Diegem, Belgium) and analyzed using ImageJ open-source software (National Institutes of Health, Bethesda, MD, USA). Quantitative analysis was performed on well-defined sagittal vibratome sections at 1.32 mm lateral from bregma, stained for W02, ThioS, AT8, NeuN, Iba1, CD68, TSPO, LAMP1, GSK3 β and Gallyas silver. The stained area relative to the total area of the image was quantified. Hippocampal area was measured on NeuN immunostained sections by delineating the brain structure and measuring the absolute surface area of the brain structure on 5 \times digital images using Image J software. Furthermore, neuronal count was performed in the CA1 region (by counting the number of NeuN stained nuclei), as well as CA1 thickness. For plaque characterization and dystrophic neurites count, a single squared area of the frontal cortex was analyzed. Plaques were outlined to measure plaque count and area. Subsequently, dystrophic neurites within the plaques were quantified and normalized for plaque area per plaque. Analysis was performed using Image J software. Confocal images were made on the Zeiss LSM900 Airyscan 2 microscope (Zeiss, Oberkochen, Germany) with a 63 \times /1.40 Oil DIC M26 objective (Zeiss). Airyscan processing was performed in ZEN blue software and z-stacks were processed with ImageJ.

Biochemical analysis

Tau aggregate concentrations in total brain homogenates were measured using the homogeneous time resolved fluorescence (HTRF) tau aggregation kit (6FtauPEG, Revvity, Waltham MA, USA), following the manufacturer protocol. Briefly, after 20 h incubation of total brain homogenates of F^{+T+} ApoE WT and F^{+T+} ApoE KO mice with the anti-tau-d2 antibody and anti-tau-tb antibody at room temperature in a low-volume 96-well plate (Revvity), the signals were measured with the CLARIOstar Plus (BMG Labtech, Ortenberg, Germany). The levels of aggregated tau (Delta F%) were calculated and normalized. Serum Neurofilament Light levels were measured on serum samples of F^{+T+} ApoE WT, F^{+T+} ApoE KO, F^{-T-} ApoE WT and F^{-T-} ApoE KO mice using the MSD R-PLEX Human Neurofilament L assay (K1517XR-2), following the manufacturer's protocol,

using the MesoScale Discovery (MSD) platform Quickplex SQ120 (Rockville, MD, USA). Sarkosyl insoluble fractions were extracted as previously described [89–91]. Cortical brain tissue was homogenized in 6 volumes of buffer and centrifuged at 100.000 g for 1 h. The pellet was resuspended in buffer including 0.8 M NaCl and again centrifuged at 15.000 g for 30 min. Sarkosyl was added to the supernatant and left for 1 h at room temperature, before centrifuging at 100.000 g for 1 h. The pellet containing the sarkosyl insoluble fraction was resuspended in PBS. For western blot, total homogenates and sarkosyl insoluble fractions were diluted appropriately in sample buffer for 7.5% Tris-Glycine gels (BioRad, California, USA). Proteins were transferred to polyvinylidene fluoride (PVDF) membranes (Merck Millipore, Burlington, MA, USA). Membranes were blocked and incubated with anti-phospho-tau (Ser202, Thr205), anti-phospho-tau (Thr212, Ser214), anti-phospho-tau (Thr181) and anti-tau monoclonal antibodies, (respectively AT8 (MN1020), AT100 (MN1060), AT270 (MN1050) and HT7 (MN1000); Thermo Fisher Scientific, Waltham, MA, USA). Afterwards they were incubated in horseradish peroxidase labeled secondary antibody (P0447; Dako, Agilent; Santa Clara, USA) before visualizing the bands with Pierce enhanced chemiluminescence (ECL) (Thermo Fisher Scientific, Waltham, MA, USA) on Amersham Imager 680 (GE Healthcare, UK). Quantification was performed using Image J software. Measurement of insoluble A β 42 and A β 40 concentration in the brain, after formic acid extraction, were performed using the INNOTEST Fujirebio ELISA (Fujirebio Diagnostics, Malvern, PA, USA) following the manufacturer's protocol. Reading was performed using the CLARIOstar Plus (BMG Labtech, Ortenberg, Germany).

Brain microglia isolation and single-cell sequencing

All processing and tissue-collection was performed as previously described [77], using the Act-Seq method [92] to limit dissociation-induced gene expression. Briefly, brains of F^{-T-} , F^{+T+} ApoE WT and F^{+T+} ApoE KO mice ($n = 6$ per group, 6 months old) were pooled, cut into small pieces, and incubated with enzyme mix (30 U/ml DNase I (Roche), 10 U/ml collagenase type I (Worthington) and 400 U/ml collagenase type IV (Worthington) diluted in HBSS with 15 μ M ActD at 11 °C for 40 min, with regular resuspension for full tissue dissociation. The solution was resuspended, filtered twice over a 100 μ m nylon filter and centrifuged at 400 g for 10 min. The pellet was resuspended in 5 ml 70% standard isotonic Percoll (SIP, GE Healthcare) diluted in 1 \times HBSS and gently overlaid with 5 ml of 30% SIP, followed by a 5 ml layer of 30% SIP, forming a three-layered density gradient (centrifuged at 650 \times g, 4 °C, 30 min without acceleration/braking). All gradient buffers contained 3 μ M ActD. The cell cloud at the 70/30% interphase was collected, centrifuged, and resuspended in staining buffer (2 mM EDTA, 2% FCS in 1 \times HBSS). Subsequently, cells were incubated with anti-mouse CD16/CD32 (clone 2.4G2), anti-CD45-Pacific Blue (clone 30-F11; BioLegend; San Diego, California, USA) CD11b-AF647 (clone M1/70; BioLegend; San Diego, California, USA) for 20 min on ice. CD45^{low}CD11b⁺ immune cells were sorted into 100% FCS using a BD FACS ARIA II with a sorting nozzle of 85 μ m. Library preparations for the single cell RNA-seq was performed using 10 \times Genomics Chromium Single Cell 3' Kit, v3.1 NextGEM chemistry (10 \times Genomics; Pleasanton, California, USA). The cell count and the viability of the samples were accessed using LUNA dual fluorescence cell counter (Logos Biosystems) and a targeted cell recovery of 2000–5000 cells were aimed for each of the samples. Post cell count and QC, the samples were immediately loaded onto the Chromium Controller. Single cell RNAseq libraries were prepared using manufacturers recommendations (Single cell 3' reagent kits v3.1 user guide; CG000204 Rev D), and at the different check points the library quality was accessed using Qubit (Thermo Fisher Scientific, Waltham, MA, USA) and Bioanalyzer (Agilent; Santa Clara, USA). For a targeted sequencing saturation of 50–60%, sequencing were performed at a depth of 30,000–40,000 reads per cell and single cell libraries were sequenced on Illumina's NovaSeq 6000 platform using paired-end sequencing workflow and with recommended 10 \times ; v3.1 read parameters (28–8–0–91 cycles). The Cell Ranger pipeline (10 \times Genomics; Pleasanton, California, USA) was used to perform sample demultiplexing and to generate FASTQ files for read 0, read 2 and the i7 sample index. Read 2, containing the cDNA, was mapped to the reference genome (mouse mm10) using STAR. Subsequent barcode processing, unique molecular identifiers filtering and single-cell 3' gene counting was performed using the Cell Ranger suite and Seurat v3.0.1. The total number of cells across all libraries was 8056 cells. The average of the mean reads per cell across all libraries was 22268. Digital gene expression matrices were preprocessed and filtered using the Scater R

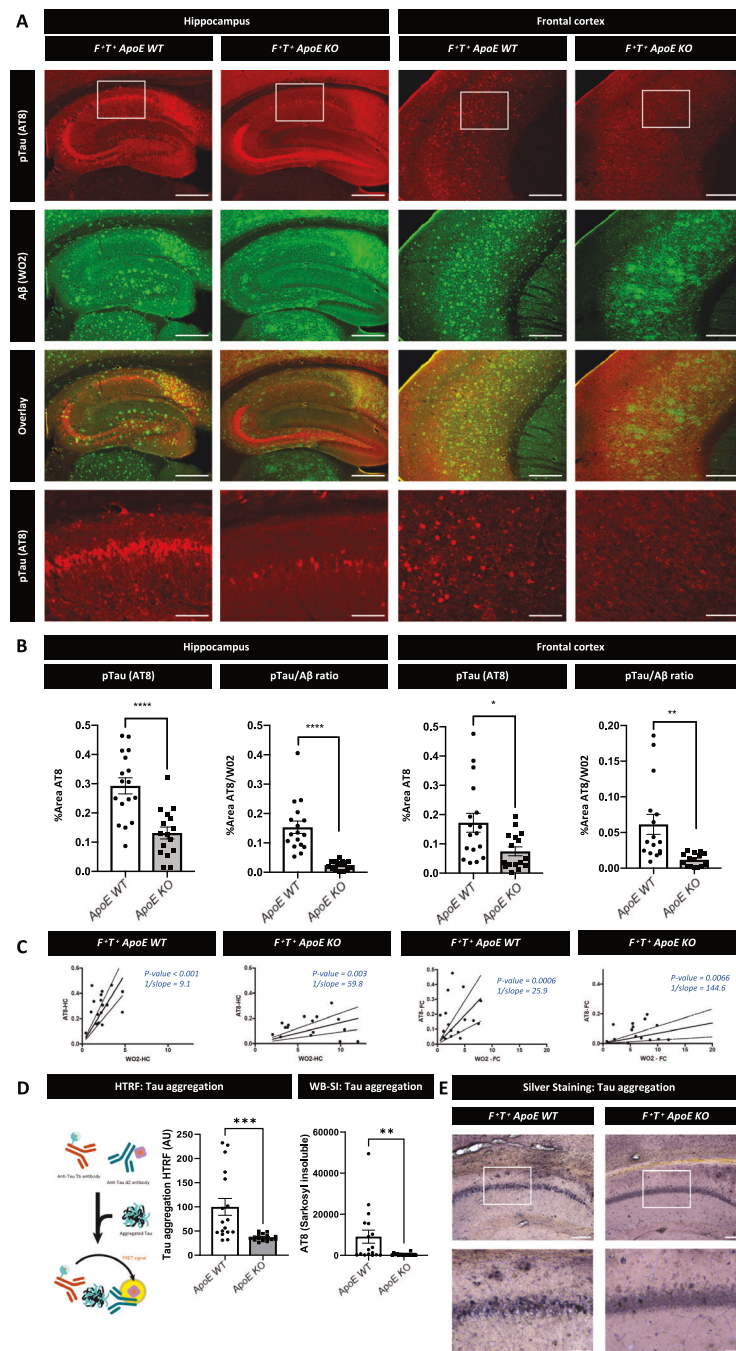


Fig. 2 APOE deficiency inhibited amyloid-facilitated tau pathology in hippocampus and frontal cortex in an ATN model. **A** Representative images of the hippocampus and frontal cortex of $F^{+}T^{+}$ ApoE WT and $F^{+}T^{+}$ ApoE KO mice stained with AT8 and W02 antibody, respectively staining p-tau pathology (top and bottom row), A β load (second row), and overlay (third row), showing a pronounced decrease in AT8 stained area in $F^{+}T^{+}$ ApoE KO compared to $F^{+}T^{+}$ ApoE WT mice. Bottom row shows higher magnification of p-tau pathology. Scalebar represents 500 μ m (top rows) and 125 μ m (bottom row). **B** Quantitative analysis of AT8 stained area in the hippocampus (left) and frontal cortex (right) of $F^{+}T^{+}$ ApoE WT ($n = 17$) and $F^{+}T^{+}$ ApoE KO ($n = 16$) mice, and of the ratio of AT8 stained area over W02 stained area in the hippocampus (left) and frontal cortex (right) of $F^{+}T^{+}$ ApoE WT ($n = 17$) and $F^{+}T^{+}$ ApoE KO ($n = 16$) mice. Following normality testing unpaired student t-test was used. Results were presented as mean \pm standard error (SEM). * $p < 0.05$, ** $p < 0.01$, **** $p < 0.0001$. **C** Linear regression analysis between W02 stained area and AT8 stained area in frontal cortex and hippocampus, respectively, reveals a more than 5 times steeper slope in $F^{+}T^{+}$ ApoE WT compared to $F^{+}T^{+}$ ApoE KO brains (1/slope is respectively 9.1 in $F^{+}T^{+}$ ApoE WT ($p < 0.001$) vs 59.8 in $F^{+}T^{+}$ ApoE KO ($p = 0.003$) in hippocampus, and 25.9 in $F^{+}T^{+}$ ApoE WT ($p = 0.0006$) vs 144.6 in $F^{+}T^{+}$ ApoE KO ($p = 0.0066$) in frontal cortex ($F^{+}T^{+}$ ApoE WT; $n = 17$; $F^{+}T^{+}$ ApoE KO; $n = 16$). **D** Schematic overview of Homogenous Time Resolved Fluorescence (HTRF) assay to detect tau aggregates (left). Quantitative analysis of tau aggregation using HTRF assay of homogenates of $F^{+}T^{+}$ ApoE WT ($n = 17$) and $F^{+}T^{+}$ ApoE KO ($n = 16$) mice (middle). Quantitative analysis of sarkosyl insoluble tau (using AT8 staining p-tau^{S202, T205}), in sarkosyl insoluble fraction of homogenates of $F^{+}T^{+}$ ApoE WT ($n = 17$) and $F^{+}T^{+}$ ApoE KO ($n = 16$) mice. Following normality testing Mann-Whitney test was used. Results were presented as mean \pm standard error (SEM). ** $p < 0.01$, *** $p < 0.001$ (right). Detailed analysis of p-tau and total tau in sarkosyl insoluble fractions and total homogenates is presented in Fig. S3. **E** Representative images of Gallyas silver staining in the CA1 region of the hippocampus (top) and zoom in of the neuronal layer (bottom) of $F^{+}T^{+}$ ApoE WT and $F^{+}T^{+}$ ApoE KO mice, showing less neurofibrillary tangles (NFTs) in APOE deficient mice. Detailed analysis of NFT staining (Gallyas silver and pFTAA) is presented in Fig. S3. Scalebar represents 100 μ m (top) and 30 μ m (bottom). WB-SI western blot – sarkosyl insoluble.

packages [93]. Data normalization and further downstream processing was performed using Seurat package in R.

Statistical analysis

Data were statistically analyzed using GraphPad Prism version 9.0 (GraphPad Software Inc, San Diego, USA). Normal distribution was tested using Shapiro–Wilk test and the data were further analyzed using unpaired t-test. For non-normally distributed data, non-parametric Mann–Whitney analysis was used, for normally distributed data unpaired parametric t-test was used. Data were analyzed using one-way analysis of variance (ANOVA) with Dunnett's test for multiple comparison for normally distributed data, or Kruskal–Wallis test with Dunn's multiple comparison test for non-normally distributed data. Variance was similar between compared groups. Sections with an artefact precluding quantitative analysis (e.g. missing or damaged parts) were removed from quantitative analysis. Outliers identified using GraphPad Prism using ROUT 1% were removed from the analysis to avoid skewing of the data by outliers. Results were presented as mean \pm standard error (SEM). A p-value of $p < 0.05$ was considered significant. * $p < 0.05$, ** $p < 0.01$, *** $p < 0.001$, **** $p < 0.0001$. Linear regression analysis was performed using GraphPad Prism version 9.0 (GraphPad Software Inc, San Diego, USA). The curve and 95% confidence interval were depicted on the graph, and the slope (and 1/slope) of the best fit were calculated and depicted on the graphs. A p-value of $p < 0.05$ was considered significant. * $p < 0.05$, ** $p < 0.01$, *** $p < 0.001$, **** $p < 0.0001$.

RESULTS

APOE deficiency inhibited amyloid-facilitated tau pathology in a preclinical ATN model

The role of APOE in AD and ATN progression, i.e. amyloid-facilitated tau pathology and associated neurodegeneration, was investigated using a model recapitulating progressive ATN pathologies, generated by crossing 5x*FAD* mice (F^{+} , expressing mutant *APP* and *PS1*) and *TauP301S* (*PS19*) mice (T^{+} , expressing mutant *Tau*), further denoted as $F^{+}T^{+}$ mice [48, 50]. This model displays strongly aggravated and accelerated tau pathology in the presence of amyloid pathology (Fig. 1A–D, Fig. S1A, B), in line with models generated by others [49, 51, 52, 94–98], highlighting reproducibility of amyloid-facilitated tau pathology. Accelerated and aggravated tau pathology in presence of amyloid pathology is proven by comparison of $F^{+}T^{+}$ mice (*APP/PS1xTau*) with the parental T^{+} mice (*Tau* only) devoid of amyloid pathology. Amyloid pathology starts to develop in $F^{+}T^{+}$ mice by the age of 3 months progressively increasing in hippocampus and cortex, reaching plateau levels at 6 months (Fig. 1E, F, Fig. S1A). $F^{+}T^{+}$ mice display a robust amyloid-facilitated tau pathology, measured by AT8 staining both in cortex and hippocampus, followed by neurodegeneration (using NeuN staining), not detected in age matched 6 months old T^{+} only mice ($F^{-}T^{+}$) in absence of amyloid pathology (Fig. 1A–D, Fig. S1B, C). In the T^{+} only mice, at the age of 6 months, no tau pathology nor atrophy is detected (Fig. S1B, C). Gallyas silver staining corroborated NFT formation in $F^{+}T^{+}$ at 6 months, absent in age-matched parental T^{+} mice (Fig. S1D, E). In the single T^{+} mice, tau pathology is detected at the age of 11 months old, followed by atrophy, while absent at 6 months of age (Fig. S1D, E, Fig. S3C). This robust acceleration and aggravation of tau pathology provides a robust ATN model, and analytical window for analyzing mechanisms of amyloid-facilitated tau pathology (Fig. 1F, G) [98].

To assess the role of APOE in progressive ATN pathology development, APOE deficient mice were crossed with $F^{+}T^{+}$ mice, or ATN model. APOE deficiency was verified using Western blotting analysis, showing absence of APOE expression in brains of $F^{+}T^{+}$ *ApoE* KO compared to $F^{+}T^{+}$ *ApoE* WT mice (Fig. S2B). Amyloid-facilitated tau pathology was assessed by immunohistochemical staining with anti-p-tau AT8 staining, detecting pathological tau, revealing a significant decrease both in hippocampus and in frontal cortex in $F^{+}T^{+}$ *ApoE* KO compared to $F^{+}T^{+}$ *ApoE*

WT mice at 6 months of age (Fig. 2A, B). The ratio of tau pathology (AT8 staining) over total A β load (W02 staining), also showed a significant decrease in $F^{+}T^{+}$ *ApoE* KO compared to $F^{+}T^{+}$ *ApoE* WT mice both in hippocampus and frontal cortex, indicating that the observed decrease was not merely due to alterations (or decreased) A β load (Fig. 2B). Our data indicate that APOE deficiency significantly decreased amyloid-facilitated tau pathology in this ATN model. Interestingly, linear regression showed a significant correlation between A β load and tau pathology supporting a link between both pathologies both in $F^{+}T^{+}$ *ApoE* WT and $F^{+}T^{+}$ *ApoE* KO mice. Notably, the slope modelling this relation was more than 5-fold increased in the presence of APOE, indicating a different relation between both pathologies in the presence compared to the absence of APOE (Fig. 2C).

To assess the effect of APOE deficiency on NFTs and aggregated insoluble tau, sarkosyl insoluble tau extraction and Gallyas silver staining were used. Western blotting of sarkosyl insoluble fraction showed decreased sarkosyl insoluble tau in $F^{+}T^{+}$ *ApoE* KO compared to $F^{+}T^{+}$ *ApoE* WT mice, using total tau, and p-tau antibodies AT8, AT270 and AT100 (Fig. 2D, Fig. S3A, B). Total soluble tau was unaltered in $F^{+}T^{+}$ *ApoE* KO compared to $F^{+}T^{+}$ *ApoE* WT mice, while also soluble p-tau was decreased (Fig. S3A, B). Furthermore, Gallyas silver staining confirmed tau aggregation as NFTs in $F^{+}T^{+}$ mice and showed decreased NFTs in $F^{+}T^{+}$ *ApoE* KO compared to $F^{+}T^{+}$ *ApoE* WT mice (Fig. 2E, Fig. S3D). Gallyas silver stained NFTs were not detected in 6 months old single T^{+} mice, in contrast to 6 months old $F^{+}T^{+}$ mice and to 11 months old single T^{+} mice (Fig. S1D, Fig. S3C). We next used pTAA, a high affinity oligothiophene probe that detects filamentous tau in vivo and in cultured cells [99], further corroborating the filamentous nature of the tau pathology assessed in $F^{+}T^{+}$ mice in presence and absence of APOE (Fig. S3E). Finally, a homogeneous time resolved fluorescence (HTRF)-based assay, was used to measure aggregated tau, ranging from small to large tau aggregates. The assay is based on a fluorescence resonance energy transfer (FRET) from excitation of the HTRF donor to the HTRF acceptor, when donor and acceptor are in close proximity, generating a specific HTRF signal, proportional to the amount of tau aggregates, including smaller and larger tau aggregates [47, 100–102]. HTRF signal was significantly lower in $F^{+}T^{+}$ *ApoE* KO compared to $F^{+}T^{+}$ *ApoE* WT mice (Fig. 2D). Together the detailed analysis of insoluble, aggregated and filamentous tau, complementing the AT8 based analysis, indicates that APOE deficiency halted amyloid-facilitated tau pathology in $F^{+}T^{+}$ mice.

APOE deficiency inhibited neurodegeneration following amyloid-facilitated tau pathology in an ATN model

Next, effects of APOE deficiency on neurodegeneration associated with amyloid-facilitated tau pathology were assessed using $F^{+}T^{+}$ *ApoE* KO and $F^{+}T^{+}$ *ApoE* WT mice. Notably, $F^{+}T^{+}$ mice display significant atrophy, measured by NeuN staining, compared to the parental $F^{-}T^{+}$ which do not show tau pathology nor atrophy at 6 months of age (Fig. 1C–E). Furthermore, marked atrophy in $F^{+}T^{+}$ mice significantly correlates with the amyloid-facilitated tau pathology, indicating its close correlation with tau pathology in $F^{+}T^{+}$ mice (Fig. 1A–E, Fig. S1B, C). Effects of APOE on tau-induced hippocampal atrophy downstream of A β load were measured on NeuN stained sections using various parameters. Hippocampal area, as well as hippocampal pyramidal CA1 layer thickness was significantly increased in $F^{+}T^{+}$ *ApoE* KO compared to $F^{+}T^{+}$ *ApoE* WT mouse brains (Fig. 3A–C). Furthermore, nuclear NeuN stained area in hippocampal CA1 region and total hippocampus was significantly increased in $F^{+}T^{+}$ *ApoE* KO compared to $F^{+}T^{+}$ *ApoE* WT mice (Fig. 3A–C). Finally, neuron counts in CA1 revealed a significant higher number of neurons in absence compared to presence of APOE (Fig. 3C). Of note, to exclude the effect on hippocampal atrophy by neurodevelopmental changes in APOE

deficient mice, comparison of the parental ($F^{-/-}$) *ApoE* WT and *ApoE* KO mice was performed, showing no differences in hippocampal parameters, reflecting no neurodevelopmental atrophy or hypertrophy due to APOE deficiency (Fig. S4A–C). Next, neurodegenerative processes in absence of APOE were assessed by measuring Neurofilament Light (NfL) concentrations serving as biofluid biomarker in patients with neurodegenerative diseases and indicator of axonal injury or neuronal death in the brain. Quantitative analysis by biochemical MesoScale Discovery assay revealed a significant decreased NfL in serum of 6 months old $F^{+/+}$ *ApoE* KO versus $F^{+/+}$ *ApoE* WT mice, reflecting decreased neurodegenerative processes in absence of APOE (Fig. 3D, E). Taken together, our data indicate that APOE deficiency decreased hippocampal atrophy and neurodegeneration in $F^{+/+}$ mice, indicating an inhibitory effect on progressive ATN development by APOE deficiency.

APOE deficiency induced robust A β pathology but decreased compacted, dense core plaques

To identify the cellular and molecular mechanism of decreased pathological tau and associated neurodegeneration in absence of APOE, we investigated in first instance, quantitative and qualitative differences in amyloid burden. Firstly, we measured total A β load, using anti-A β directed W02 immunostaining to stain all A β , including diffuse amyloid plaques as well as dense core, compacted plaques. This revealed – unexpectedly – significantly increased A β load in $F^{+/+}$ *ApoE* KO compared to $F^{+/+}$ *ApoE* WT mice (Fig. 4A, B). The effect of APOE deficiency on tau pathology is hence not due to decreased total A β load. To further assess qualitative differences in A β load we performed staining with ThioS, intercalating between β -sheets and demonstrating the fibrillar nature of dense core amyloid plaques. ThioS staining revealed a significantly decreased dense core plaque load in $F^{+/+}$ *ApoE* KO compared to $F^{+/+}$ *ApoE* WT mice in hippocampus and frontal cortex (Fig. 4C, D). Also, more diffuse A β load was strikingly observed *de visu* in brains of $F^{+/+}$ *ApoE* KO mice compared to $F^{+/+}$ *ApoE* WT, and could serve as a tell-tale of APOE deficiency. The effect of APOE deficiency on the development of neuritic plaques, defined as amyloid plaques associated with dystrophic neurites, was assessed using LAMP1 staining (Fig. S5A, D) and other markers such as AT8 and GSK3 β , near amyloid plaques (Fig. S5B, C, E, F). Quantitative analysis showed decreased dystrophic neurites associated with amyloid plaques in $F^{+/+}$ *ApoE* KO compared to $F^{+/+}$ *ApoE* WT, in hippocampal and cortical brain regions using different markers (Fig. 4E, Fig. S5, D–F), together indicating altered amyloid burden. Further biochemical analysis showed no significant quantitative differences in concentrations of A β 40, A β 42, ratio A β 42/40 and total A β in formic acid or insoluble fraction of brain homogenates (Fig. S5G). Together, the combined histological and biochemical analysis indicated a qualitative shift in load without significant quantitative change, to more diffuse and less dense core amyloid pathology. Finally, qualitative differences in A β burden, were further reflected in plaque size and plaque number, showing a significant robust increase in plaque size but decrease in plaque number in $F^{+/+}$ *ApoE* KO mice compared to $F^{+/+}$ *ApoE* WT (Fig. 4F). Taken together, APOE deficiency caused a qualitative shift in amyloid pathology, by increasing total W02-stained A β load, while decreasing dense core, compacted amyloid plaques.

APOE deficiency halted microglial conversion beyond homeostatic microglia towards reactive and DAM microglia

APOE is a crucial modulator in the conversion of microglia towards a neurodegenerative microglial phenotype (MGnD) or disease associated microglial phenotype (DAM) in the context of several neurodegenerative stressors, including apoptotic neurons [57]. APOE also affects the association of microglia with amyloid

plaques in amyloid only models [40, 43, 44, 62, 103]. Here we studied APOE effects on microgliosis and microglial phenotypes in the presence of ATN pathologies. We first assessed microgliosis in the ATN model *per se*, showing strong microgliosis in $F^{+/+}$ mice displaying combined amyloid pathology, tau pathology, and neurodegeneration- compared to non-transgenic mice and single $T^{+/+}$ mice not displaying amyloid pathology ($F^{-/-}$ $T^{+/+}$ mice) (Fig. S6A–H), indicating the robust induction of microgliosis with combined ATN pathologies. Next, significantly and marked decreased microgliosis in absence of APOE, was shown by decreased Iba1 immunostaining in hippocampus and frontal cortex, of $F^{+/+}$ *ApoE* KO mice compared to $F^{+/+}$ *ApoE* WT (Fig. 5A, B, Fig. S7E–H, Fig. S8A). Higher magnification of Iba1 immunostaining, showed morphological changes revealing decreased microglial activation in absence of APOE in $F^{+/+}$ *ApoE* KO mice compared to $F^{+/+}$ *ApoE* WT mice (Fig. 5A, Fig. S7H). CD68 staining, considered as a marker for activated, phagocytosing microglia, also showed decreased activated microglia in absence of APOE (Fig. S7C, D). Finally, TSPO staining, a marker for microgliosis in the context of neurodegenerative diseases, and used for PET-based detection of microgliosis in AD patients, was decreased in $F^{+/+}$ *ApoE* KO mice compared to $F^{+/+}$ *ApoE* WT mice in hippocampus and frontal cortex (Fig. S7A, B).

To investigate effects of APOE deficiency in modulating the microglial conversion program from homeostatic towards neurodegenerative or disease associated microglia (DAM), RNA sequencing was used at single cell resolution. We performed single cell RNA-Sequencing analysis on CD45^{low}CD11b⁺ cells sorted from 6-month-old $F^{-/-}$ (hereafter referred as WT, $n = 4838$), $F^{+/+}$ *ApoE* WT ($n = 2671$) and $F^{+/+}$ *ApoE* KO ($n = 3830$). The individual samples were combined in a single dataset on which we performed unsupervised clustering and dimensionality reduction via the Uniform Manifold Approximation and Projection (UMAP) technique (Fig. 6A, B). Immune cell clusters, which included microglia, border associated macrophages (BAMs), monocytes and various lymphocyte subsets, were identified based on previously described gene expression signatures [47, 56, 57, 77]. Microglia were identified based on the expression of macrophage (e.g.: C1qa, Fcgr1, Aif1) and microglial signature genes (e.g.: Tmem119, P2ry12, Sall1) and the absence of lineage markers of other cell populations identified in the single cell suspension (Fig. 6C, E, Fig. S8B). We observed 4 main microglia subsets across the 3 experimental groups, namely homeostatic microglia, reactive microglia, DAM and interferon-signaling microglia. Importantly, the percentage of reactive and DAM microglia were significantly increased in $F^{+/+}$ *ApoE* WT brains ($p < 0.0001$, Fisher's test) compared to WT brains, displaying no ATN pathologies and mostly homeostatic microglia (Fig. 6D). Most interestingly, microglia remained mostly homeostatic in brains of $F^{+/+}$ *ApoE* KO mice (Fig. 6D), with a strong reduction in the frequency of reactive microglia ($F^{+/+}$ *ApoE* WT = 58%; $F^{+/+}$ *ApoE* KO = 2%, $p < 0.0001$) and DAM ($F^{+/+}$ *ApoE* WT = 28%; $F^{+/+}$ *ApoE* KO = 15%, $p < 0.0001$). This indicates that ATN pathology results in a global microglial activation, resulting in induction of reactive and DAM microglia, while APOE deficiency resulted in a strong maintenance of homeostatic microglia.

Taken together, APOE deficiency in $F^{+/+}$ transgenic mice decreased overall microgliosis, assessed by Iba1, CD68 and TSPO, and blocked conversion of homeostatic microglia into the DAM transitional program, resulting in increased homeostatic microglia at the expense of reactive and DAM microglia, maintaining microglia in a WT-like state.

Microglial elimination decreased amyloid-facilitated tau pathology in the presence, but not absence of APOE

To verify if microglia contributed significantly to amyloid-facilitated tau pathology in $F^{+/+}$ mice, microglia were depleted using CSF1R inhibition in the ATN model. Administration of the

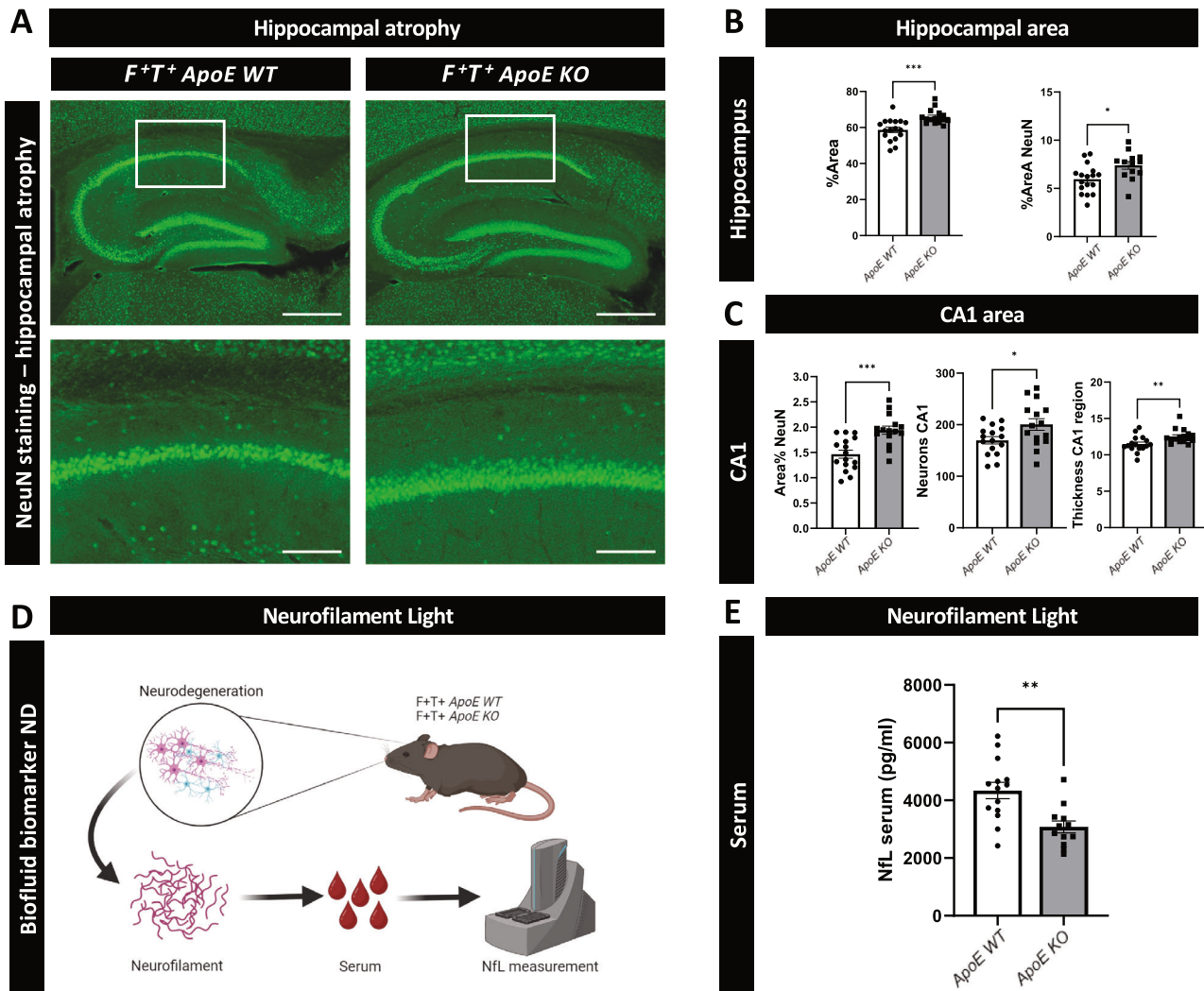


Fig. 3 APOE deficiency inhibited neurodegeneration downstream of amyloid-facilitated tau pathology in an ATN model. **A** Representative images of the hippocampus (top) and CA1 (bottom) of *F⁺T⁺ ApoE WT* and *F⁺T⁺ ApoE KO* mice stained with NeuN antibody. Scalebar represents 500 μ m (top) and 125 μ m (bottom). **B** Quantitative analysis of hippocampal area (left) and NeuN positive signal (right) in *F⁺T⁺ ApoE WT* ($n = 17$) and *F⁺T⁺ ApoE KO* ($n = 16$). **C** Quantitative analysis of NeuN positive signal in CA1 (left), number of neurons in CA1 (middle) and thickness of CA1 region (right) of *F⁺T⁺ ApoE WT* ($n = 16$) and *F⁺T⁺ ApoE KO* ($n = 15$). **D** Schematic representation of the experimental set-up of NFL measurement in serum of *F⁺T⁺ ApoE WT* and *F⁺T⁺ ApoE KO* mice. **E** Concentration of serum NFL, measured using electrochemiluminescence assay (MSD), of *F⁺T⁺ ApoE WT* ($n = 14$) and *F⁺T⁺ ApoE KO* ($n = 12$) mice. Following normality testing unpaired t-test was used for normally distributed sets, non-parametric Mann-Whitney was used for non-normally distributed data. Results were presented as mean \pm standard error (SEM). * $p < 0.05$, ** $p < 0.01$, *** $p < 0.001$. NFL: Neurofilament light chain.

CSF1R inhibitor PLX3397, from 3 to 6 months, resulted in a significant reduction of Iba1 staining in the frontal cortex and hippocampus in brains of *F⁺T⁺ ApoE WT* mice, indicating successful microglial elimination (Fig. 7D, E). In *F⁺T⁺ ApoE WT* mice, microglial elimination resulted in a strong inhibition of amyloid-facilitated tau pathology, highlighting a role of microglia in this process (Fig. 7A, B, E). Notably, PLX3397 treatment from 3–6 months in *F⁺T⁺ ApoE WT* in hippocampus significantly decreased amyloid pathology, consequently both decreased amyloid pathology and microglial elimination may contribute to the observed diminished tau pathology in the hippocampal region (Fig. 7A–C, E). In frontal cortex, however, PLX3397 treatment did not result in a significant decrease of amyloid pathology, indicating a role of microglia in amyloid-facilitated tau pathology in frontal cortex, independent of its effect on amyloid pathology (Fig. 7A–C, E). Treatment with PLX3397 in *F⁺T⁺ ApoE KO* mice showed a drastic inhibition of microglia in the frontal cortex and hippocampus (Figure S9D, E). However, microglial

elimination in *F⁺T⁺ ApoE KO* mice did not result in a significant decrease in tau pathology as seen in the *F⁺T⁺ ApoE WT* (Figure S9A, B, E). Taken together our data support a contributory APOE-related role of microglia in amyloid-facilitated tau pathology in the ATN model.

DISCUSSION

Despite promising recent successes, anti-A β therapies still remain of limited clinical benefit to patients, highlighting the need for multitargeting approaches, capable of halting ATN progression beyond A β pathology [2–7]. Herein, we assessed the effect of APOE deficiency on ATN progression in a robust preclinical ATN model. We showed that APOE deficiency inhibits progressive amyloid-driven tau pathology and neurodegeneration, despite high A β load. Our findings are remarkably reminiscent of findings in extremely resilient ADAD case reports [28–30, 32, 33, 104], which display decreased tau pathology and neurodegeneration

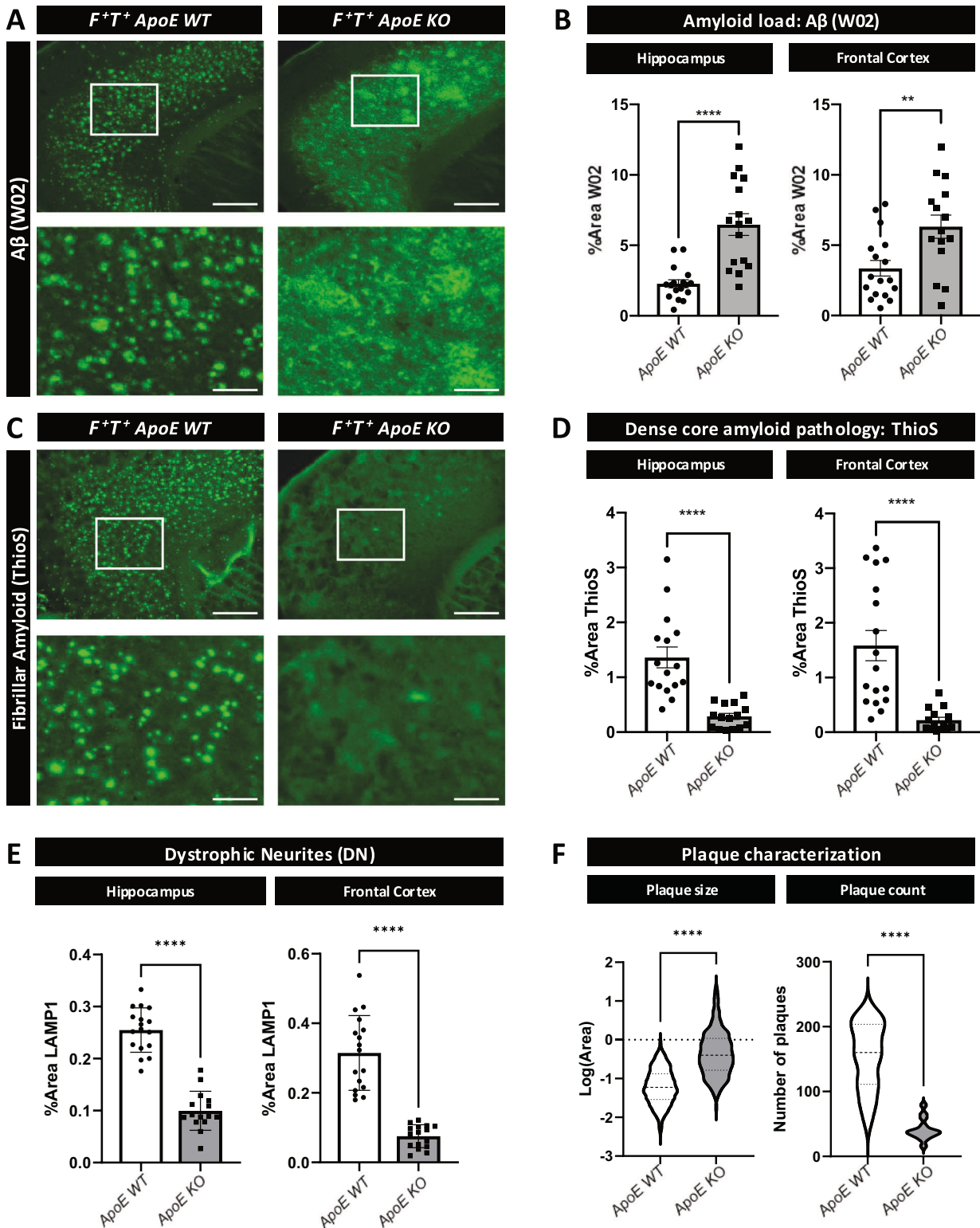


Fig. 4 APOE deficiency decreased compacted dense core plaques, despite high Aβ burden. **A** Representative images of the frontal cortex of *F⁺T⁺ ApoE WT* and *F⁺T⁺ ApoE KO* mice stained with W02 antibody (top) and higher magnification (bottom). Scalebar represents 500 μm (top) and 125 μm (bottom). **B** Quantitative analysis of W02 signal in the hippocampus and frontal cortex of *F⁺T⁺ ApoE WT* (*n* = 17) and *F⁺T⁺ ApoE KO* (*n* = 16) mice. **C** Representative images of the frontal cortex of *F⁺T⁺ ApoE WT* and *F⁺T⁺ ApoE KO* mice stained with ThioS staining. Scalebar represents 500 μm. Higher magnifications shown on bottom row (scalebar represents 125 μm). **D** Quantitative analysis of ThioS stained area in the hippocampus and frontal cortex of *F⁺T⁺ ApoE WT* (*n* = 16) and *F⁺T⁺ ApoE KO* (*n* = 15) mice. **E** Quantitative analysis of LAMP1 staining in the hippocampus and frontal cortex of *F⁺T⁺ ApoE WT* (*n* = 17) and *F⁺T⁺ ApoE KO* (*n* = 15) mice (images shown in Fig. S5A). **F** Quantitative analysis of plaque count and plaque size in the frontal cortex of *F⁺T⁺ ApoE WT* (*n* = 17) and *F⁺T⁺ ApoE KO* (*n* = 15) mice. Following normality testing unpaired t-test was used for normally distributed sets, non-parametric Mann-Whitney was used for non-normally distributed data. Results were presented as mean ± standard error (SEM). ***p* < 0.01, *****p* < 0.0001.

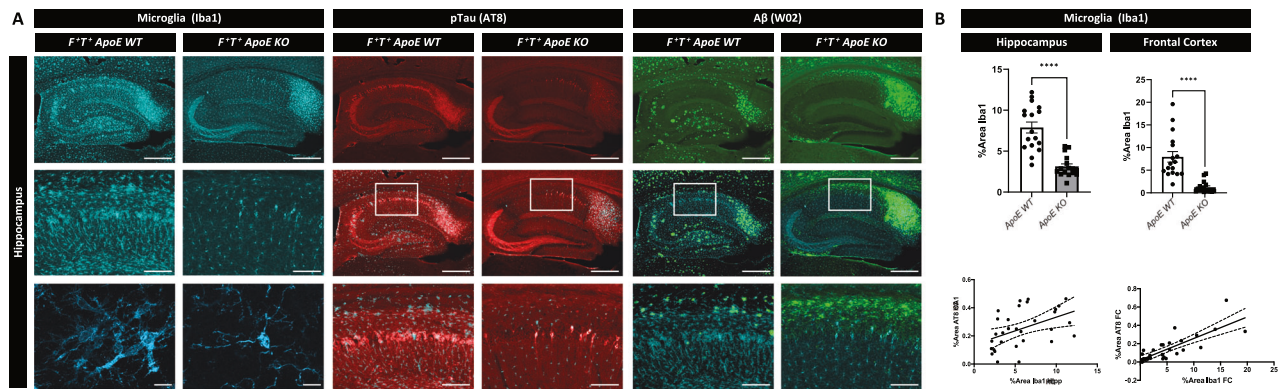


Fig. 5 APOE deficiency inhibited microgliosis in a model recapitulating ATN pathology. **A** Representative images of the hippocampus of $F^{+}T^{+}$ ApoE WT and $F^{+}T^{+}$ ApoE KO mice stained with Iba1 (left panel), AT8 (middle panel) and W02 (right panel) antibody. Top row shows hippocampus of $F^{+}T^{+}$ ApoE WT and $F^{+}T^{+}$ ApoE KO mice stained for microglia (Iba1), p-tau (AT8) and Aβ (W02). Scalebar is 500 μm. Second row of the first panel shows higher magnifications of microglia stained in the CA1 region in $F^{+}T^{+}$ ApoE WT and $F^{+}T^{+}$ ApoE KO mice. Scalebar is 125 μm. Second row of panel two and three shows overlay of microglia with respectively p-tau pathology and Aβ load in the hippocampus of $F^{+}T^{+}$ ApoE WT and $F^{+}T^{+}$ ApoE KO mice. Scalebar is 500 μm. Third row of the first panel shows high resolution confocal images of microglia in the hippocampus of $F^{+}T^{+}$ ApoE WT and $F^{+}T^{+}$ ApoE KO mice. Scalebar is 10 μm. Third row in the second and third panel show higher magnifications overlays of microglia and respectively p-tau pathology and Aβ load in the CA1 of $F^{+}T^{+}$ ApoE WT and $F^{+}T^{+}$ ApoE KO mice. Scalebar is 125 μm. **B** Quantitative analysis of Iba1 stained area in the hippocampus and frontal cortex of $F^{+}T^{+}$ ApoE WT ($n = 17$) and $F^{+}T^{+}$ ApoE KO ($n = 16$) mice (top). Linear regression analysis showed a correlation between microgliosis and p-tau pathology in hippocampus (left bottom) and frontal cortex (right bottom). Following normality testing unpaired student t-test was used. Results were presented as mean ± standard error (SEM). **** $p < 0.0001$.

despite a high Aβ load. Putative protective mutations in the APOE pathway identified in these cases support the role of APOE [3, 28–30, 32] in their observed resilience against ATN progression. The recent classification of APOE4 homozygosity as genetic AD [38], in addition to earlier identification of APOE as a major AD risk factor [34–37], further underscores the importance of the APOE-pathway in AD. Here we show that APOE deficiency favorably impacts ATN progression by multitargeting effects by (i) inhibiting compact, dense core plaque formation, without decreasing total Aβ burden in this model and (ii) inhibiting homeostatic microglia phenotypic conversion, associated with (iii) inhibiting amyloid-facilitated tau pathology and neurodegeneration.

APOE deficiency inhibits amyloid-facilitated tau pathology and neurodegeneration in a robust preclinical ATN model

The various AD stages are referred to as the ATN continuum [9, 11–15]. Amyloid pathology develops up to a decade prior to progressive spread of tau pathology beyond the entorhinal cortex [12, 15, 16], associated with neurodegeneration and symptom development [8, 17, 18]. ADAD mutations altering Aβ biogenesis and enhancing Aβ accumulation in the brain, invariably –exemptive of exceptional high resilience ADAD cases with putative protective mutations– cause progressive tau pathology along with progressive neurodegeneration and symptoms [19–21]. This indicates a causal link and interrelations between amyloid and progressive tau pathology associated with neurodegeneration, although details of the mechanistic links remain incompletely understood –in terms of toxic Aβ culprits and pathways–, preventing effective therapeutic development. Nevertheless, these mechanisms represent a core feature of AD development, since individuals with amyloid pathology only display mild cognitive impairment. And most importantly, while anti-Aβ clinical trials robustly and strongly decrease Aβ load, tau pathology and neurodegeneration are ineffectively impacted requiring better understanding of the interrelation between ATN pathologies.

Preclinical studies have captured amyloid-facilitated tau pathology [47, 49, 51, 52, 94–96]. Previous studies showed that Aβ facilitates tau seeding near amyloid plaques [105] as tau pathology in dystrophic neurites, eventually spreading to the soma leading to initiation of tangle formation, and representing a compelling mechanism for early amyloid-driven tau pathology seeding

[105, 106]. However, this model did not mimic the later-phase of robust neurofibrillary tangle formation nor associated neurodegeneration. Herein, we used a robust model that recapitulates strong late-stage amyloid-facilitated tau pathology, including robust, somatodendritic tau accumulation and NFT pathology, and tau-associated neurodegeneration [7, 47–50]. Using this model, we show that amyloid pathology substantially precedes tau pathology, and most importantly very potently aggravates and accelerates tau-associated pathology and neurodegeneration [7, 47–50], recapitulating ATN progression. However, it is important to note that artificial combined overexpression of mutant APP, PS1 and MAPT used in the ATN model does not exist in humans. Along this vein, it must be noted that similar artificial models using combined overexpression of mutant APP and PS1, not existing in humans, did provide the basis for successful removal of amyloid pathology in current immunotherapies in the clinic [2–6]. Similarly, –artificial–models recapitulating robust ATN pathologies, could provide the basis for developing strategies for halting ATN progression, while taking their limitations into consideration. The presented model develops a very robust ATN pathology, with a large window for mechanistic analysis, and closely resembles the temporal sequence of the ATN continuum seen in human AD patients. The generated ATN model provides a robust, invaluable tool to mechanistically study and therapeutic target ATN progression.

During early-stage ATN, APOE4 immunotherapy mitigates Aβ-facilitated tau seeding, increasing dystrophic neurites near plaques in a mouse amyloidosis model expressing human APOE4 [45]. Importantly, also the APOE3Chch mutation was recently and elegantly shown to inhibit early Aβ-facilitated tau seeding in dystrophic neurites, validating its protective effect and supporting an APOE role in this process [31]. However, effects on amyloid-facilitated robust tau pathology and tau-associated neurodegeneration were not assessed in this model. Here, we show that APOE deficiency mitigates late amyloid-facilitated tau pathology and downstream tau-induced neurodegeneration. We here found that APOE deficiency inhibited ATN progression, associated with decreasing dense core Aβ plaque formation and blocking conversion of homeostatic microglia to reactive and DAM states, as outlined in detail below. Besides its effects on microglia and dense core plaque formation halting ATN pathologies, APOE may modulate Aβ-induced TN pathologies by alternative mechanisms [62, 107]. These may include altered APOE-Aβ interaction affecting

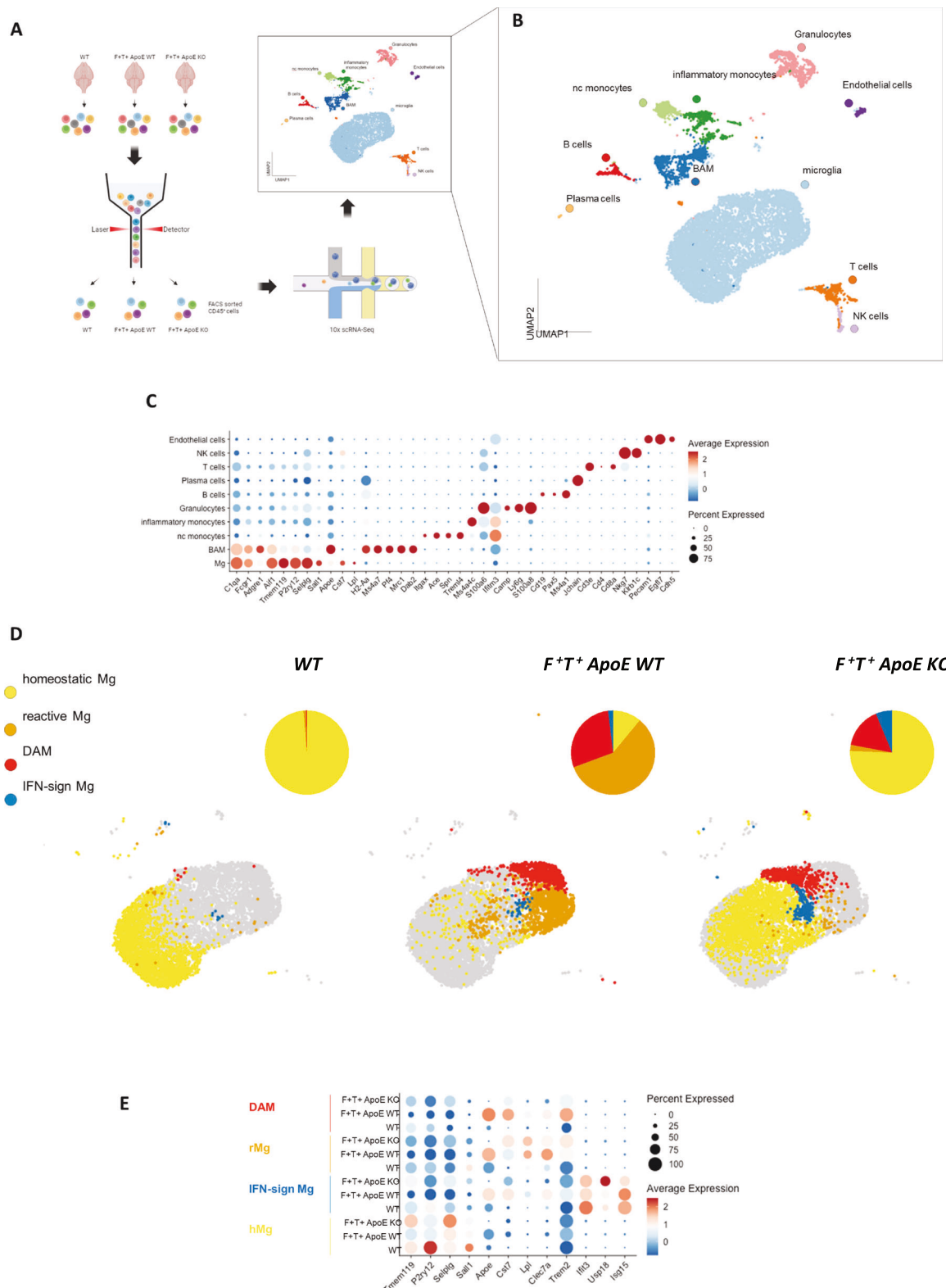


Fig. 6 APOE deficiency halted conversion of homeostatic microglia in an ATN model. **A** Schematic overview representing the single cell RNA-sequencing setup used for WT, F^{+T+} ApoE WT and F^{+T+} ApoE KO brain isolation ($n = 6$ per genotype), single cell isolation, sequencing and analysis. **B** UMAP-projection of cells analysed (WT = 4838, F^{+T+} ApoE WT = 2671, F^{+T+} ApoE KO = 3830). nc monocytes: nonclassical monocytes. **C** Dot plot visualizing expression of key marker genes for each of the clusters that were identified in **B**. **D** UMAP projection of the microglia cluster in their respective experimental groups showing different microglial phenotypes: homeostatic microglia (hMg, yellow), reactive microglia (rMg, orange), disease-associated microglia (DAM, red) and interferon-signalling microglia (IFN-sign Mg, blue). Only coloured cells belong to the specified condition, cells belonging to other conditions are depicted in grey. The pie charts represent the percentages of the 4 distinct microglia subsets, within total microglia, per condition. **E** Dot plot representing the expression of signature genes for the different microglial genotypes.

A β aggregation, in addition to potential microglial contributions [62, 107, 108]. Alternatively, APOE may alter ATN pathologies by impacting binding with HSPGs and APOE receptors, including with LRP [53, 54], involved in tau seed uptake [54], or by affecting Reelin binding to APOER2 and VLDL receptors directly impacting tau-phosphorylation [55]. These direct effects on tau pathology, in addition to the observed effects on amyloid burden and microglia, must be considered as potential additional contributors of decreased tau pathology and neurodegeneration. These APOE-dependent effects may cumulatively contribute to its overall beneficial effects on ATN progression. Here, in this work we unequivocally show that APOE deficiency halts ATN progression by pleiotropic, multitargeting effects, including (i) inhibiting compacted, neuritic plaque pathology, without decreasing total A β load, (ii) inhibiting microglia phenotypic conversion beyond homeostatic microglia, resulting in (iii) inhibiting amyloid-driven tau-pathology and neurodegeneration.

APOE deficiency mitigates formation of compacted fibrillar amyloid plaques in a preclinical ATN model, despite high A β load

APOE affects amyloid pathology in amyloid-only models by altering A β -clearance, amyloid plaque seeding [28, 39], plaque compaction, and microglial association with plaques [32, 37, 39–44, 62, 87, 109]. However, the effect of APOE deficiency on subsequent late-stage tau pathology and tau-induced neurodegeneration remained unexplored. Here, we strikingly –serving as ‘*de visu*’ tell-tale for genotype– recapitulate APOE deficiency promoting diffuse A β and blocking compacted and fibrillar amyloid plaque formation, despite high A β load. Qualitative differences were observed in absence of quantitative differences in total A β concentrations. Our data are strongly in line with previous publications, while subtle differences may relate to the models or strategies used [43, 44, 109, 110]. However, APOE deficiency may induce pleiotropic actions, including impacting APOE–A β interaction, A β aggregation, APOE-dependent microglial phenotypes involved in A β clearance, seed formation and plaque compaction, and APOE-dependent effects via APOE-receptors, competing with A β binding, or APOE-dependent effects on lipids, requiring follow-up to pinpoint the mechanisms involved. We here extend prior literature by reporting that APOE deficiency mitigates induction of late-stage somatodendritic p-tau pathology and subsequent neurodegeneration, despite high A β load. The findings are in line with the association of compacted neuritic plaques, in contrast to diffuse plaques, with neuronal loss and cognitive decline in AD [9, 111–113]. Our data support A β species associated with mature dense core plaque formation, including oligomeric species [22, 24], as toxic culprits linked to microgliosis in the induction of A β -triggered tau pathology and subsequent neurodegeneration, processes known to be associated with symptom development in AD. Overall, here, we show that APOE deficiency inhibits robust amyloid-driven tau pathology, late-stage somatodendritic tau pathology, and associated neurodegeneration –processes linked with symptom development in AD–, associated with blocking dense core plaque formation despite high amyloid load.

APOE deficiency halts progression beyond homeostatic microglia in a preclinical ATN model

APOE plays a key role in microglial phenotypes [58, 62, 104, 114] and microgliosis is a core AD feature related to neurodegenerative diseases [7, 57, 59–62]. Microglia modulate the neurodegenerative disease process through potentially protective and detrimental contributions [7, 57, 59–62], determined by surrounding pathogenic cues, including ATN pathologies. Among these processes is the ability of microglia to influence amyloid and tau pathology independently, as well as dually through amyloid-driven tau pathology with consequent neurodegeneration. In the context of

neurodegenerative diseases, microglial phenotypes convert from a homeostatic resting state to reactive and DAM states [56, 57, 77], but identifying resilience factors against microglial conversion may constitute a potential therapeutic strategy. APOE and TREM2 are a critical axis in the transition towards the DAM phenotype [56, 57]. We now show, in the context of ATN pathology, APOE deficiency blocks the transition from homeostatic microglia towards a reactive or DAM phenotype, resembling more to a microglia signature reminiscent of non-transgenic mice. We previously showed that amyloid-facilitated tau pathology accelerates this microglial transition program, associated with increased APOE expression [47]. Therefore, APOE deficiency-mediated blockade of this program presents an attractive avenue to alter microglial phenotype, halting ATN progression or as a potential therapeutic target.

Microglia actively contribute to amyloid-facilitated tau pathology and neurodegeneration in a preclinical ATN model

To further assess the role of microglia on progressive ATN pathology, we eliminated microglia in our model in the presence and absence of APOE. We found that eliminating microglia decreased amyloid-facilitated tau pathology in APOE-expressing mice. In frontal cortex, eliminating microglia did not significantly reduce amyloid load per se, indicating that microglia modulate amyloid-driven tau pathology in the presence of APOE. In hippocampus, microglial elimination significantly decreased amyloid burden, in line with previous findings, dependent on amyloid stage [115], but precluding firm conclusions on their role on amyloid-facilitated tau pathology per se. Interestingly, eliminating microglia to a certain threshold has also been shown to decrease tau pathology in primary tauopathy models lacking amyloid pathology [75, 116]. Eliminating microglia mitigates APOE4 exacerbated tau pathology and tau-induced neurodegeneration in a tauopathy model lacking amyloid pathology [40, 72] supporting direct microglial modulation of tau pathology and neurodegeneration. Here we demonstrate that eliminating microglia reduces amyloid-facilitated tau pathology in APOE-expressing mice despite high amyloid burden. Eliminating microglia from APOE deficient mice did not impact tau pathology, suggesting APOE-dependent microglial modulation. Therefore, microglia modulate cross-talk between amyloid pathology and progressive late-stage TN pathology in an APOE-dependent manner, implicating microglial conversion beyond homeostatic microglia in ATN progression. This highlights the importance of microglial APOE, even though astrocytes are the main producers of APOE in physiological conditions in the brain [117]. Notably, also non-microglial processes, described above, including APOE-receptor dependent signaling pathways, may additionally contribute to the observed effects on tau pathology. Together our data support a contributory role of APOE and microglia in the late-stage of amyloid-driven tau pathology associated with neurodegeneration.

APOE as therapeutic target to halt amyloid-facilitated tau pathology and neurodegeneration, and target different AD stages

Our data indicate that targeting APOE may potentially mitigate AD progression, including inhibiting progression to late-stage amyloid-driven tau pathology and neurodegeneration, advocating APOE as a target for halting progressive ATN development. The putative protective APOE3*Chch* mutation [29–32], and its prevention of early A β -facilitated tau seeding, further supports this notion, as does the discovery of the *RELN-COLBOS* mutation, which may similarly be protective against amyloid-driven tau pathology [30, 43, 76]. Alternative protective APOE mutations, including APOE3 *Jacksonville* (V236E) [28], add to the growing body of evidence implicating APOE pathways in ATN progression.

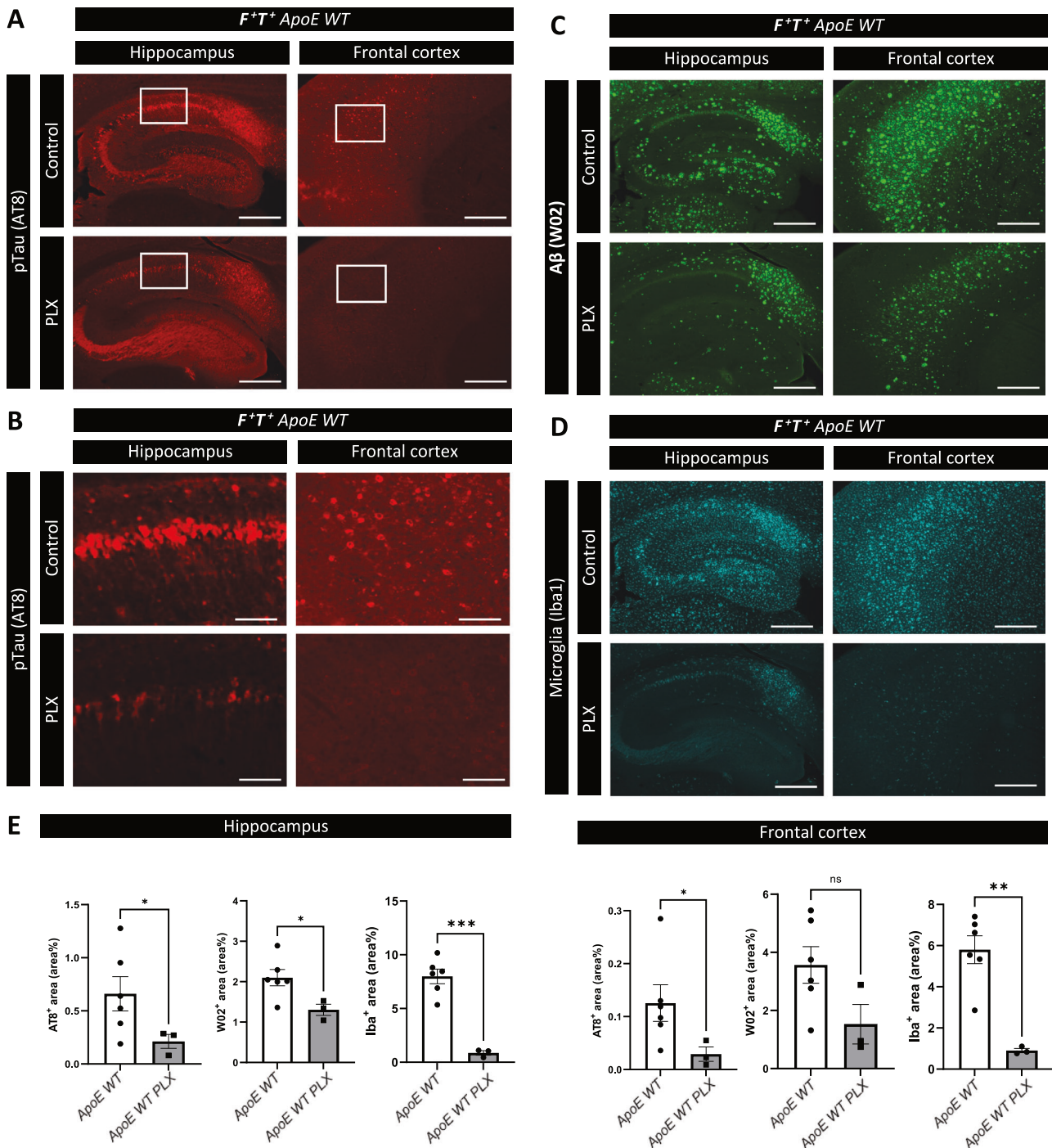


Fig. 7 Microglia elimination inhibited amyloid-driven tau pathology in hippocampus and frontal cortex in the presence of APOE but not in absence of APOE. **A** Representative images of p-tau pathology (AT8) in the hippocampus and frontal cortex of PLX treated and control *F⁺T⁺ ApoE WT* mice. Scalebar is 500 μ m. **B** Higher magnification of CA1 region and frontal cortex of the images in **A**. Scalebar is 125 μ m. **C** Representative images of A β pathology (W02) in the hippocampus and frontal cortex of PLX treated and control *F⁺T⁺ ApoE WT* mice. Scalebar is 500 μ m. **D** Representative images of microglia (Iba1) in the hippocampus and frontal cortex of PLX treated and control *F⁺T⁺ ApoE WT* mice. Scalebar is 500 μ m. **E** Quantitative analysis of p-tau pathology (AT8), A β pathology (W02) and microglia (Iba1) in hippocampus and frontal cortex of PLX3397 treated ($n = 3$) and control ($n = 6$) *F⁺T⁺ ApoE WT* mice. Following normality testing unpaired student t-test was used. Data are presented as mean \pm SEM; * $p < 0.05$, ** $p < 0.01$, *** $p < 0.001$. The analysis of microglial elimination using PLX3397 treatment in *F⁺T⁺ ApoE KO* mice is presented in Fig. S9, showing no significant effect on amyloid-facilitated tau pathology in absence of APOE.

Interestingly, our data further support the inhibiting effects of APOE or APOE4 immunization against amyloid pathology or the initial phase associated with early tau seeding near amyloid plaques [118–120]. Moreover, our data build on the previously shown therapeutic potential of APOE modulation of amyloid

and tau pathology independently, while now demonstrating decreased amyloid-facilitated tau pathology and associated neurodegeneration, in line with putative protective APOE pathway mutants. We here demonstrate that APOE deficiency inhibits development of late-stage ATN pathology development, which is

critical as halting these processes downstream of amyloid pathology will be critical to stop symptom development and progression. Noteworthy, timing of the intervention is important to consider for therapy. We here show, that genetic deletion of ApoE -starting before birth-, inhibits tau pathology and neurodegeneration downstream of amyloid, implying that early treatment could be required for successful halting of ATN pathologies. These findings are in line with the putative protective APOE pathway mutations found in human subjects. Furthermore, Huynh et al. showed that reducing APOE levels through anti-sense oligonucleotide (ASO) therapy was more effective in the prepathological stage, further showing the importance of the timing and a putative preventive nature of APOE therapies [108]. Further research is required to pinpoint or differentiate preventive and/or curative effects of APOE, while the observed decreased tau pathology following microglial elimination may suggest potential additional beneficial effects of microglial/APOE modulation in later stages, following presence of amyloid pathology. In conclusion, inhibiting APOE functions, potentially induced by immunotherapy, ASO therapy or alternative modalities may present as interesting avenues, while timing of intervention needs to be carefully considered. It is important to note, here, that we targeted the murine *ApoE* gene, which provided important novel insights. With the murine APOE mostly resembling human APOE4, the observed effects may relate to deficiency of the more detrimental APOE4 isoform rather than APOE in general [38]. Further validation of APOE as a therapeutic target will include validation in models using different human APOE isoforms. Nevertheless, in sum, our results advocate for further study of APOE along with detailed underlying mechanisms to leverage APOE related therapeutic opportunity for AD.

CONCLUSION

Overall, using a robust model of ATN pathology, we show that APOE deficiency decreased progression of late-stage amyloid-facilitated tau pathology and consequent neurodegeneration, despite high A β load. These findings are reminiscent of the high resilience ADAD case reports with putative protective mutations in the APOE pathway. The observed effects of APOE deficiency on ATN progression were associated with reduced dense core plaque formation, favoring large diffuse A β deposits, and blocked transition of homeostatic microglia to the reactive and DAM phenotype. Moreover, microglial elimination significantly decreased amyloid-driven tau pathology in the presence of APOE. Taken together, our data indicate that APOE deficiency inhibits ATN progression by pleiotropic effects, including inhibition of dense core amyloid plaque formation, and inhibition of microglial conversion beyond homeostatic microglia, while our findings also lend support to the validation of protective APOE mutations. Our data also advocate APOE as a potential therapeutic AD target although validation in different models will be important, unlocking promising avenues for its further detailed therapeutic exploration.

DATA AVAILABILITY

Data will be available upon reasonable request to the corresponding author.

REFERENCES

- Alzheimer's Disease International 2018. The state of the art of dementia research: new frontiers. World Alzheimer Report; London; 2018.
- Knopman DS. Lecanemab reduces brain amyloid-beta and delays cognitive worsening. *Cell Rep Med*. 2023;4:100982. <https://doi.org/10.1016/j.xcrm.2023.100982>.
- van Dyck CH, Swanson CJ, Aisen P, Bateman RJ, Chen C, Gee M, et al. Lecanemab in early Alzheimer's disease. *N Engl J Med*. 2023;388:9–21. <https://doi.org/10.1056/NEJMoa2212948>.
- Sims JR, Zimmer JA, Evans CD, Lu M, Ardayfio P, Sparks J, et al. Donanemab in early symptomatic Alzheimer disease: The TRAILBLAZER-ALZ 2 randomized clinical trial. *JAMA*. 2023;330:512–27. <https://doi.org/10.1001/jama.2023.13239>.
- Boxer AL, Sperling R. Accelerating Alzheimer's therapeutic development: the past and future of clinical trials. *Cell*. 2023;186:4757–72. <https://doi.org/10.1016/j.cell.2023.09.023>.
- Jucker M, Walker LC. Alzheimer's disease: from immunotherapy to immunoprevention. *Cell*. 2023;186:4260–70. <https://doi.org/10.1016/j.cell.2023.08.021>.
- Wilson DM 3rd, Cookson MR, Van Den Bosch L, Zetterberg H, Holtzman DM, Dewachter I. Hallmarks of neurodegenerative diseases. *Cell*. 2023;186:693–714. <https://doi.org/10.1016/j.cell.2022.12.032>.
- Braak H, Braak E. Neuropathological staging of Alzheimer-related changes. *Acta Neuropathol*. 1991;82:239–59. <https://doi.org/10.1007/bf00308809>.
- Serrano-Pozo A, Frosch MP, Masliah E, Hyman BT. Neuropathological alterations in Alzheimer disease. *Cold Spring Harb Perspect Med*. 2011;1:a006189. <https://doi.org/10.1101/cshperspect.a006189>.
- Thal DR, Rub U, Orantes M, Braak H. Phases of A beta-deposition in the human brain and its relevance for the development of AD. *Neurology*. 2002;58:1791–1800. <https://doi.org/10.1212/wnl.58.12.1791>.
- Hyman BT, Phelps CH, Beach TG, Bigio EH, Cairns NJ, Carrillo MC, et al. National institute on aging-Alzheimer's association guidelines for the neuropathologic assessment of Alzheimer's disease. *Alzheimers Dement*. 2012;8:1–13. <https://doi.org/10.1016/j.jalz.2011.10.007>.
- Jack CR Jr, Bennett DA, Blennow K, Carrillo MC, Dunn B, Haeberlein SB, et al. NIA-AA research framework: toward a biological definition of Alzheimer's disease. *Alzheimers Dement*. 2018;14:535–62. <https://doi.org/10.1016/j.jalz.2018.02.018>.
- Jack CR Jr, Bennett DA, Blennow K, Carrillo MC, Feldman HH, Frisone GB, et al. A/T/N: An unbiased descriptive classification scheme for Alzheimer disease biomarkers. *Neurology*. 2016;87:539–47. <https://doi.org/10.1212/wnl.0000000000002923>.
- Jack CR Jr, Knopman DS, Jagust WJ, Petersen RC, Weiner MW, Aisen PS, et al. Tracking pathophysiological processes in Alzheimer's disease: an updated hypothetical model of dynamic biomarkers. *Lancet Neurol*. 2013;12:207–16. [https://doi.org/10.1016/S1474-4422\(12\)70291-0](https://doi.org/10.1016/S1474-4422(12)70291-0).
- Hanseeuw BJ, Betensky RA, Jacobs HIL, Schultz AP, Sepulcre J, Becker JA, et al. Association of amyloid and tau with cognition in preclinical Alzheimer disease: A longitudinal study. *JAMA Neurol*. 2019;76:915–24. <https://doi.org/10.1001/jamaneurol.2019.1424>.
- Bateman RJ, Xiong C, Benzinger TL, Fagan AM, Goate A, Fox NC, et al. Clinical and biomarker changes in dominantly inherited Alzheimer's disease. *N Engl J Med*. 2012;367:795–804. <https://doi.org/10.1056/NEJMoa1202753>.
- Pascoal TA, Benedet AL, Tudorascu DL, Theriault J, Mathotaarachchi S, Savard M, et al. Longitudinal 18F-MK-6240 tau tangles accumulation follows Braak stages. *Brain*. 2021;144:3517–28. <https://doi.org/10.1093/brain/awab248>.
- Xia C, Makarets SJ, Caso C, McGinnis S, Gomperts SN, Sepulcre J, et al. Association of in vivo [18F]AV-1451 tau PET imaging results with cortical atrophy and symptoms in typical and atypical Alzheimer disease. *JAMA Neurol*. 2017;74:427–36. <https://doi.org/10.1001/jamaneurol.2016.5755>.
- Hardy J, Selkoe DJ. The amyloid hypothesis of Alzheimer's disease: progress and problems on the road to therapeutics. *Science*. 2002;297:353–6. <https://doi.org/10.1126/science.1072994>.
- Long JM, Holtzman DM. Alzheimer disease: an update on pathobiology and treatment strategies. *Cell*. 2019;179:312–39. <https://doi.org/10.1016/j.cell.2019.09.001>.
- Musiek ES, Holtzman DM. Three dimensions of the amyloid hypothesis: time, space and 'wingmen'. *Nat Neurosci*. 2015;18:800–6. <https://doi.org/10.1038/nn.4018>.
- Bhatt N, Kaye R. Quantification and targeting of elusive neurotoxic amyloid oligomers. *Cell Rep Med*. 2022;3:100636. <https://doi.org/10.1016/j.xcrm.2022.100636>.
- Kass B, Schemmert S, Zafiu C, Pils M, Bannach O, Kutzsche J, et al. Abeta oligomer concentration in mouse and human brain and its drug-induced reduction ex vivo. *Cell Rep Med*. 2022;3:100630. <https://doi.org/10.1016/j.xcrm.2022.100630>.
- Sengupta U, Nilson AN, Kaye R. The role of amyloid-beta oligomers in toxicity, propagation, and immunotherapy. *EBioMedicine*. 2016;6:42–9. <https://doi.org/10.1016/j.ebiom.2016.03.035>.
- Ghag G, Bhatt N, Cantu DV, Guerrero-Munoz MJ, Ellsworth A, Sengupta U, et al. Soluble tau aggregates, not large fibrils, are the toxic species that display seeding and cross-seeding behavior. *Protein Sci*. 2018;27:1901–9. <https://doi.org/10.1002/pro.3499>.
- Lesne S, Koh MT, Kotilinek L, Kaye R, Glabe CG, Yang A, et al. A specific amyloid-beta protein assembly in the brain impairs memory. *Nature*. 2006;440:352–7. <https://doi.org/10.1038/nature04533>.
- Kaye R, Head E, Thompson JL, McIntire TM, Milton SC, Cotman CW, et al. Common structure of soluble amyloid oligomers implies common mechanism of pathogenesis. *Science*. 2003;300:486–9. <https://doi.org/10.1126/science.1079469>.
- Liu CC, Murray ME, Li X, Zhao N, Wang N, Heckman MG, et al. APOE3-Jacksonville (V236E) variant reduces self-aggregation and risk of dementia. *Sci Transl Med*. 2021;13:eabc9375. <https://doi.org/10.1126/scitranslmed.abc9375>.

29. Arboleda-Velasquez JF, Lopera F, O'Hare M, Delgado-Tirado S, Marino C, Chmielewska N, et al. Resistance to autosomal dominant Alzheimer's disease in an APOE3 Christchurch homozygote: a case report. *Nat Med*. 2019;25:1680–3. <https://doi.org/10.1038/s41591-019-0611-3>.
30. Zalcusky KA, Nelson MR, Huang Y. An Alzheimer's-disease-protective APOE mutation. *Nat Med*. 2019;25:1648–9. <https://doi.org/10.1038/s41591-019-0634-9>.
31. Chen Y, Song S, Parhizkar S, Lord J, Zhu Y, Strickland MR, et al. APOE3 alters microglial response and suppresses Abeta-induced tau seeding and spread. *Cell*. 2024;187:428–45.e420. <https://doi.org/10.1016/j.cell.2023.11.029>.
32. Lopera F, Marino C, Chandras AS, O'Hare M, Villalba-Moreno ND, Aguillon D, et al. Resilience to autosomal dominant Alzheimer's disease in a Reelin-COLBO heterozygous man. *Nat Med*. 2023;29:1243–52. <https://doi.org/10.1038/s41591-023-02318-3>.
33. Moufofo EN, Spire-Jones TL. Reeling from news that reelin defends the brain against Alzheimer's. *Cell Rep Med*. 2023;4:101111. <https://doi.org/10.1016/j.xcrm.2023.101111>.
34. Corder EH, Saunders AM, Strittmatter WJ, Schmechel DE, Gaskell PC, Small GW, et al. Gene dose of apolipoprotein E type 4 allele and the risk of Alzheimer's disease in late onset families. *Science*. 1993;261:921–3. <https://doi.org/10.1126/science.8346443>.
35. Abraham R, Moskvina V, Sims R, Hollingworth P, Morgan A, Georgieva L, et al. A genome-wide association study for late-onset Alzheimer's disease using DNA pooling. *BMC Med Genomics*. 2008;1:44. <https://doi.org/10.1186/1755-8794-1-44>.
36. Harold D, Abraham R, Hollingworth P, Sims R, Gerrish A, Hamshere ML, et al. Genome-wide association study identifies variants at CLU and PICALM associated with Alzheimer's disease. *Nat Genet*. 2009;41:1088–93. <https://doi.org/10.1038/ng.440>.
37. Mahan TE, Wang C, Bao X, Choudhury A, Ulrich JD, Holtzman DM. Selective reduction of astrocyte apoE3 and apoE4 strongly reduces Aβ accumulation and plaque-related pathology in a mouse model of amyloidosis. *Mol Neurodegener*. 2022;17:13. <https://doi.org/10.1186/s13024-022-00516-0>.
38. Fortea J, Pegueroles J, Alcolea D, Belbin O, Dols-Icardo O, Vaque-Alcazar L, et al. APOE4 homozygosity represents a distinct genetic form of Alzheimer's disease. *Nat Med*. 2024;30:1284–91. <https://doi.org/10.1038/s41591-024-02931-w>.
39. Liu CC, Zhao N, Fu Y, Wang N, Linares C, Tsai CW, et al. ApoE4 accelerates early seeding of amyloid pathology. *Neuron*. 2017;96:1024–32.e1023. <https://doi.org/10.1016/j.neuron.2017.11.013>.
40. Shi Y, Yamada K, Liddell SA, Smith ST, Zhao L, Luo W, et al. ApoE4 markedly exacerbates tau-mediated neurodegeneration in a mouse model of tauopathy. *Nature*. 2017;549:523–7. <https://doi.org/10.1038/nature24016>.
41. Wang C, Xiong M, Gratzke M, Bao X, Shi Y, Andhey PS, et al. Selective removal of astrocytic APOE4 strongly protects against tau-mediated neurodegeneration and decreases synaptic phagocytosis by microglia. *Neuron*. 2021;109:1657–74.e1657. <https://doi.org/10.1016/j.neuron.2021.03.024>.
42. Christensen DZ, Schneider-Axmann T, Lucassen PJ, Bayer TA, Wirths O. Accumulation of intraneuronal Aβ correlates with ApoE4 genotype. *Acta Neuropathol*. 2010;119:555–66. <https://doi.org/10.1007/s00401-010-0666-1>.
43. Holtzman DM, Fagan AM, Mackey B, Tenkova T, Sartorius L, Paul SM, et al. Apolipoprotein E facilitates neuritic and cerebrovascular plaque formation in an Alzheimer's disease model. *Ann Neurol*. 2000;47:739–47.
44. Ulrich JD, Ulland TK, Mahan TE, Nystrom S, Nilsson KP, Song WM, et al. ApoE facilitates the microglial response to amyloid plaque pathology. *J Exp Med*. 2018;215:1047–58. <https://doi.org/10.1084/jem.20171265>.
45. Wang C, Nambiar A, Strickland MR, Lee C, Parhizkar S, Moore AC, et al. APOE-ε4 synergizes with sleep disruption to accelerate Abeta deposition and Abeta-associated tau seeding and spreading. *J Clin Invest*. 2023. <https://doi.org/10.1172/JCI169131>.
46. Nelson MR, Liu P, Agrawal A, Yip O, Blumenfeld J, Traglia M, et al. The APOE-R136S mutation protects against APOE4-driven tau pathology, neurodegeneration and neuroinflammation. *Nat Neurosci*. 2023;26:2104–21. <https://doi.org/10.1038/s41593-023-01480-8>.
47. Lodder C, Scheyltjens I, Stancu IC, Botella Lucena P, Gutierrez de Rave M, Vanherle S, et al. CSF1R inhibition rescues tau pathology and neurodegeneration in an A/T/N model with combined AD pathologies, while preserving plaque associated microglia. *Acta Neuropathol Commun*. 2021;9:108. <https://doi.org/10.1186/s40478-021-01204-8>.
48. Oakley H, Cole SL, Logan S, Maus E, Shao P, Craft J, et al. Intraneuronal beta-amyloid aggregates, neurodegeneration, and neuron loss in transgenic mice with five familial Alzheimer's disease mutations: potential factors in amyloid plaque formation. *J Neurosci*. 2006;26:10129–40. <https://doi.org/10.1523/JNEUROSCI.1202-06.2006>.
49. Stancu IC, Ris L, Vasconcelos B, Marinangeli C, Goeminne L, Laporte V, et al. Tauopathy contributes to synaptic and cognitive deficits in a murine model for Alzheimer's disease. *FASEB J*. 2014;28:2620–31. <https://doi.org/10.1096/fj.13-246702>.
50. Yoshiyama Y, Higuchi M, Zhang B, Huang SM, Iwata N, Saido TC, et al. Synapse loss and microglial activation precede tangles in a P301S tauopathy mouse model. *Neuron*. 2007;53:337–51. <https://doi.org/10.1016/j.neuron.2007.01.010>.
51. Pooler AM, Polydoro M, Maury EA, Nicholls SB, Reddy SM, Wegmann S, et al. Amyloid accelerates tau propagation and toxicity in a model of early Alzheimer's disease. *Acta Neuropathol Commun*. 2015;3:14. <https://doi.org/10.1186/s40478-015-0199-x>.
52. Li T, Braunstein KE, Zhang J, Lau A, Sibener L, Deeb C, et al. The neuritic plaque facilitates pathological conversion of tau in an Alzheimer's disease mouse model. *Nat Commun*. 2016;7:12082. <https://doi.org/10.1038/ncomms12082>.
53. Beisiegel U, Weber W, Ihrke G, Herz J, Stanley KK. The LDL-receptor-related protein, LRP, is an apolipoprotein E-binding protein. *Nature*. 1989;341:162–4. <https://doi.org/10.1038/341162a0>.
54. Rauch JN, Luna G, Guzman E, Audouard M, Challis C, Sibih YE, et al. LRP1 is a master regulator of tau uptake and spread. *Nature*. 2020;580:381–5. <https://doi.org/10.1038/s41586-020-2156-5>.
55. Hiesberger T, Trommsdorff M, Howell BW, Goffinet A, Mumby MC, Cooper JA, et al. Direct binding of Reelin to VLDL receptor and ApoE receptor 2 induces tyrosine phosphorylation of disabled-1 and modulates tau phosphorylation. *Neuron*. 1999;24:481–9. [https://doi.org/10.1016/s0896-6273\(00\)80861-2](https://doi.org/10.1016/s0896-6273(00)80861-2).
56. Keren-Shaul H, Spinrad A, Weiner A, Matcovitch-Natan O, Dvir-Szternfeld R, Ulland TK, et al. A unique microglia type associated with restricting development of Alzheimer's disease. *Cell*. 2017;169:1276–90.e1217. <https://doi.org/10.1016/j.cell.2017.05.018>.
57. Krasemann S, Madore C, Cialic R, Baufeld C, Calcagno N, El Fatimy R, et al. The TREM2-APOE pathway drives the transcriptional phenotype of dysfunctional microglia in neurodegenerative diseases. *Immunity*. 2017;47:566–81.e569. <https://doi.org/10.1016/j.immuni.2017.08.008>.
58. Paolicelli RC, Sierra A, Stevens B, Tremblay ME, Aguzzi A, Ajami B, et al. Microglia states and nomenclature: a field at its crossroads. *Neuron*. 2022;110:3458–83. <https://doi.org/10.1016/j.neuron.2022.10.020>.
59. Heneka MT, Carson MJ, El Khoury J, Landreth GE, Brosseron F, Feinstein DL, et al. Neuroinflammation in Alzheimer's disease. *Lancet Neurol*. 2015;14:388–405. [https://doi.org/10.1016/S1474-4422\(15\)70016-5](https://doi.org/10.1016/S1474-4422(15)70016-5).
60. Heneka MT, Golenbock DT, Latz E. Innate immunity in Alzheimer's disease. *Nat Immunol*. 2015;16:229–36. <https://doi.org/10.1038/ni.3102>.
61. Ransohoff RM. How neuroinflammation contributes to neurodegeneration. *Science*. 2016;353:777–83. <https://doi.org/10.1126/science.aag2590>.
62. Shi Y, Holtzman DM. Interplay between innate immunity and Alzheimer disease: APOE and TREM2 in the spotlight. *Nat Rev Immunol*. 2018;18:759–72. <https://doi.org/10.1038/s41577-018-0051-1>.
63. Martens YA, Zhao N, Liu CC, Kanekiyo T, Yang AJ, Goate AM, et al. ApoE cascade hypothesis in the pathogenesis of Alzheimer's disease and related dementias. *Neuron*. 2022;110:1304–17. <https://doi.org/10.1016/j.neuron.2022.03.004>.
64. Chen Y, Strickland MR, Soranno A, Holtzman DM. Apolipoprotein E: structural insights and links to Alzheimer disease pathogenesis. *Neuron*. 2021;109:205–21. <https://doi.org/10.1016/j.neuron.2020.10.008>.
65. Fernandez-Calle R, Konings SC, Frontinan-Rubio J, Campubi-Ferrer L, Svensson M, et al. APOE in the bullseye of neurodegenerative diseases: impact of the APOE genotype in Alzheimer's disease pathology and brain diseases. *Mol Neurodegener*. 2022;17:62. <https://doi.org/10.1186/s13024-022-00566-4>.
66. Bellucci A, Bugiani O, Ghetti B, Spillantini MG. Presence of reactive microglia and neuroinflammatory mediators in a case of frontotemporal dementia with P301S mutation. *Neurodegener Dis*. 2011;8:221–9. <https://doi.org/10.1159/000322228>.
67. Bellucci A, Westwood AJ, Ingram E, Casamenti F, Goedert M, Spillantini MG. Induction of inflammatory mediators and microglial activation in mice transgenic for mutant human P301S tau protein. *Am J Pathol*. 2004;165:1643–52. [https://doi.org/10.1016/S0002-9440\(10\)63421-9](https://doi.org/10.1016/S0002-9440(10)63421-9).
68. Bevan-Jones WR, Cope TE, Jones PS, Kaalund SS, Passamonti L, Allinson K, et al. Neuroinflammation and protein aggregation co-localize across the frontotemporal dementia spectrum. *Brain*. 2020;143:1010–26. <https://doi.org/10.1093/brain/awaa033>.
69. Dani M, Wood M, Mizoguchi R, Fan Z, Walker Z, Morgan R, et al. Microglial activation correlates in vivo with both tau and amyloid in Alzheimer's disease. *Brain*. 2018;141:2740–54. <https://doi.org/10.1093/brain/awy188>.
70. Ismail R, Parbo P, Madsen LS, Hansen AK, Hansen KV, Schaldemose JL, et al. The relationships between neuroinflammation, beta-amyloid and tau deposition in Alzheimer's disease: a longitudinal PET study. *J Neuroinflammation*. 2020;17:151. <https://doi.org/10.1186/s12974-020-01820-6>.
71. Pascoal TA, Benedet AL, Ashton NJ, Kang MS, Theriault J, Chamoun M, et al. Microglial activation and tau propagate jointly across Braak stages. *Nat Med*. 2021;27:1592–9. <https://doi.org/10.1038/s41591-021-01456-w>.

72. Shi Y, Manis M, Long J, Wang K, Sullivan PM, Remolina Serrano J, et al. Microglia drive APOE-dependent neurodegeneration in a tauopathy mouse model. *J Exp Med*. 2019;216:2546–61. <https://doi.org/10.1084/jem.20190980>.
73. Stancu IC, Cremers N, Vanrusselt H, Couturier J, Vanoosthuyse A, Kessels S, et al. Aggregated tau activates NLRP3-ASC inflammasome exacerbating exogenously seeded and non-exogenously seeded tau pathology in vivo. *Acta Neuropathol*. 2019;137:599–617. <https://doi.org/10.1007/s00401-018-01957-y>.
74. Ising C, Venegas C, Zhang S, Scheiblich H, Schmidt SV, Vieira-Saecker A, et al. NLRP3 inflammasome activation drives tau pathology. *Nature*. 2019;575:669–73. <https://doi.org/10.1038/s41586-019-1769-z>.
75. Mancuso R, Fryatt G, Cleal M, Obst J, Pipi E, Monzon-Sandoval J, et al. CSF1R inhibitor JNJ-40346527 attenuates microglial proliferation and neurodegeneration in P301S mice. *Brain*. 2019;142:3243–64. <https://doi.org/10.1093/brain/awz241>.
76. Kang SS, Ebbert MTW, Baker KE, Cook C, Wang X, Sens JP, et al. Microglial translational profiling reveals a convergent APOE pathway from aging, amyloid, and tau. *J Exp Med*. 2018;215:2235–45. <https://doi.org/10.1084/jem.20180653>.
77. Van Hove H, Martens L, Scheyltjens I, De Vlaminck K, Pombo Antunes AR, De Prijck S, et al. A single-cell atlas of mouse brain macrophages reveals unique transcriptional identities shaped by ontogeny and tissue environment. *Nat Neurosci*. 2019;22:1021–35. <https://doi.org/10.1038/s41593-019-0393-4>.
78. Kunkle BW, Grenier-Boley B, Sims R, Bis JC, Damotte V, Naj AC, et al. Genetic meta-analysis of diagnosed Alzheimer's disease identifies new risk loci and implicates Abeta, tau, immunity and lipid processing. *Nat Genet*. 2019;51:414–30. <https://doi.org/10.1038/s41588-019-0358-2>.
79. Sims R, Hill M, Williams J. The multiplex model of the genetics of Alzheimer's disease. *Nat Neurosci*. 2020;23:311–22. <https://doi.org/10.1038/s41593-020-0599-5>.
80. Botella Lucena P, Vanherle S, Lodder C, Gutierrez de Rave M, Stancu IC, Lambrichts I, et al. Blood-based Abeta42 increases in the earliest pre-pathological stage before decreasing with progressive amyloid pathology in preclinical models and human subjects: opening new avenues for prevention. *Acta Neuropathol*. 2022;144:489–508. <https://doi.org/10.1007/s00401-022-02458-9>.
81. McInnes J, Wierda K, Snellinx A, Bounti L, Wang YC, Stancu IC, et al. Synaptogyrin-3 mediates presynaptic dysfunction induced by tau. *Neuron*. 2018;97:823–35.e828. <https://doi.org/10.1016/j.neuron.2018.01.022>.
82. Vasconcelos B, Stancu IC, Buist A, Bird M, Wang P, Vanoosthuyse A, et al. Heterotypic seeding of tau fibrillization by pre-aggregated Abeta provides potent seeds for prion-like seeding and propagation of tau-pathology in vivo. *Acta Neuropathol*. 2016;131:549–69. <https://doi.org/10.1007/s00401-015-1525-x>.
83. Wang P, Joberty G, Buist A, Vanoosthuyse A, Stancu IC, Vasconcelos B, et al. Tau interactome mapping based identification of Otub1 as tau deubiquitinase involved in accumulation of pathological Tau forms in vitro and in vivo. *Acta Neuropathol*. 2017;133:731–49. <https://doi.org/10.1007/s00401-016-1663-9>.
84. Zhang B, Carroll J, Trojanowski JQ, Yao Y, Iba M, Potuzak JS, et al. The microtubule-stabilizing agent, epothilone D, reduces axonal dysfunction, neurotoxicity, cognitive deficits, and Alzheimer-like pathology in an interventional study with aged tau transgenic mice. *J Neurosci*. 2012;32:3601–11. <https://doi.org/10.1523/JNEUROSCI.4922-11.2012>.
85. Iba M, Guo JL, McBride JD, Zhang B, Trojanowski JQ, Lee VM. Synthetic tau fibrils mediate transmission of neurofibrillary tangles in a transgenic mouse model of Alzheimer's-like tauopathy. *J Neurosci*. 2013;33:1024–37. <https://doi.org/10.1523/JNEUROSCI.2642-12.2013>.
86. Gotz J, Deters N, Doldissen A, Bokhari L, Ke Y, Wiesner A, et al. A decade of tau transgenic animal models and beyond. *Brain Pathol*. 2007;17:91–103. <https://doi.org/10.1111/j.1750-3639.2007.00051.x>.
87. Castillo-Carranza DL, Gerson JE, Sengupta U, Guerrero-Munoz MJ, Lasagna-Reeves CA, Kaye R. Specific targeting of tau oligomers in Htau mice prevents cognitive impairment and tau toxicity following injection with brain-derived tau oligomeric seeds. *J Alzheimers Dis*. 2014;40:S97–S111. <https://doi.org/10.3233/JAD-132477>.
88. Soto-Faguas CM, Sanchez-Molina P, Saura CA. Loss of presenilin function enhances tau phosphorylation and aggregation in mice. *Acta Neuropathol Commun*. 2021;9:162. <https://doi.org/10.1186/s40478-021-01259-7>.
89. Terwel D, Muyliaert D, Dewachter I, Borghgraef P, Croes S, Devijver H, et al. Amyloid activates GSK-3beta to aggravate neuronal tauopathy in bigenic mice. *Am J Pathol*. 2008;172:786–98. <https://doi.org/10.2353/ajpath.2008.070904>.
90. Stancu IC, Vasconcelos B, Ris L, Wang P, Villers A, Peeraer E, et al. Templated misfolding of tau by prion-like seeding along neuronal connections impairs neuronal network function and associated behavioral outcomes in tau transgenic mice. *Acta Neuropathol*. 2015;129:875–94. <https://doi.org/10.1007/s00401-015-1413-4>.
91. Terwel D, Lasrado R, Snauwaert J, Vandeweert E, Van Haesendonck C, Borghgraef P, et al. Changed conformation of mutant tau-P301L underlies the moribund tauopathy, absent in progressive, nonlethal axonopathy of tau-4R/2N transgenic mice. *J Biol Chem*. 2005;280:3963–73. <https://doi.org/10.1074/jbc.M409876200>.
92. Wu YE, Pan L, Zuo Y, Li X, Hong W. Detecting activated cell populations using single-cell RNA-seq. *Neuron*. 2017;96:313–29.e316. <https://doi.org/10.1016/j.neuron.2017.09.026>.
93. Lun AT, McCarthy DJ, Marioni JC. A step-by-step workflow for low-level analysis of single-cell RNA-seq data with bioconductor. *F1000Res*. 2016;5:2122. <https://doi.org/10.12688/f1000research.9501.2>.
94. Bolmont T, Clavaguera F, Meyer-Luehmann M, Herzog MC, Radde R, Staufenbiel M, et al. Induction of tau pathology by intracerebral infusion of amyloid-beta-containing brain extract and by amyloid-beta deposition in APP x tau transgenic mice. *Am J Pathol*. 2007;171:2012–20. <https://doi.org/10.2353/ajpath.2007.070403>.
95. Gotz J, Chen F, van Dorpe J, Nitsch RM. Formation of neurofibrillary tangles in P301 tau transgenic mice induced by Abeta 42 fibrils. *Science*. 2001;293:1491–5. <https://doi.org/10.1126/science.1062097>.
96. Hurtado DE, Molina-Porcel L, Iba M, Aboagye AK, Paul SM, Trojanowski JQ, et al. Abeta accelerates the spatiotemporal progression of tau pathology and augments tau amyloidosis in an Alzheimer mouse model. *Am J Pathol*. 2010;177:1977–88. <https://doi.org/10.2353/ajpath.2010.100346>.
97. Lewis J, Dickson DW, Lin WL, Chisholm L, Corral A, Jones G, et al. Enhanced neurofibrillary degeneration in transgenic mice expressing mutant tau and APP. *Science*. 2001;293:1487–91. <https://doi.org/10.1126/science.1058189>.
98. Stancu IC, Vasconcelos B, Terwel D, Dewachter I. Models of beta-amyloid induced tau-pathology: the long and "folded" road to understand the mechanism. *Mol Neurodegener*. 2014;9:51. <https://doi.org/10.1186/1750-1326-9-51>.
99. Brelstaff J, Ossola B, Neher JJ, Klingstedt T, Nilsson KP, Goedert M, et al. The fluorescent pentameric oligothiophene pTAA identifies filamentous tau in live neurons cultured from adult P301S tau mice. *Front Neurosci*. 2015;9:184. <https://doi.org/10.3389/fnins.2015.00184>.
100. Ben-Yehuda H, Arad M, Peralta Ramos JM, Sharon E, Castellani G, Ferrera S, et al. Key role of the CCR2-CCL2 axis in disease modification in a mouse model of tauopathy. *Mol Neurodegener*. 2021;16:39. <https://doi.org/10.1186/s13024-021-00458-z>.
101. Romano LEL, Aw WY, Hixson KM, Novoselova TV, Havener TM, Howell S, et al. Multi-omic profiling reveals the ataxia protein saccin is required for integrin trafficking and synaptic organization. *Cell Rep*. 2022;41:111580. <https://doi.org/10.1016/j.celrep.2022.111580>.
102. Stancu IC, Lodder C, Botella Lucena P, Vanherle S, Gutierrez de Rave M, Terwel D, et al. The NLRP3 inflammasome modulates tau pathology and neurodegeneration in a tauopathy model. *Glia*. 2022;70:1117–32. <https://doi.org/10.1002/glia.24160>.
103. Holtzman DM, Bales KR, Tenkova T, Fagan AM, Parsadanian M, Sartorius LJ, et al. Apolipoprotein E isoform-dependent amyloid deposition and neuritic degeneration in a mouse model of Alzheimer's disease. *Proc Natl Acad Sci USA*. 2000;97:2892–7. <https://doi.org/10.1073/pnas.050004797>.
104. Liu CC, Liu CC, Kanekiyo T, Xu H, Bu G. Apolipoprotein E and Alzheimer disease: risk, mechanisms and therapy. *Nat Rev Neurol*. 2013;9:106–18. <https://doi.org/10.1038/nrneurol.2012.263>.
105. He Z, Guo JL, McBride JD, Narasimhan S, Kim H, Changolkar L, et al. Amyloid-beta plaques enhance Alzheimer's brain tau-seeded pathologies by facilitating neuritic plaque tau aggregation. *Nat Med*. 2018;24:29–38. <https://doi.org/10.1038/nm.4443>.
106. Vergara C, Houben S, Suain V, Yilmaz Z, De Decker R, Vanden Dries V, et al. Amyloid-beta pathology enhances pathological fibrillary tau seeding induced by Alzheimer PHF in vivo. *Acta Neuropathol*. 2019;137:397–412. <https://doi.org/10.1007/s00401-018-1953-5>.
107. Kanekiyo T, Xu H, Bu G. ApoE and Abeta in Alzheimer's disease: accidental encounters or partners? *Neuron*. 2014;81:740–54. <https://doi.org/10.1016/j.neuron.2014.01.045>.
108. Huynh TV, Liao F, Francis CM, Robinson GO, Serrano JR, Jiang H, et al. Age-dependent effects of apoE reduction using antisense oligonucleotides in a model of beta-amyloidosis. *Neuron*. 2017;96:1013–23.e1014. <https://doi.org/10.1016/j.neuron.2017.11.014>.
109. Liu S, Breitbart A, Sun Y, Mehta PD, Boutajangout A, Scholtzova H, et al. Blocking the apolipoprotein E/amyloid beta interaction in triple transgenic mice ameliorates Alzheimer's disease related amyloid beta and tau pathology. *J Neurochem*. 2014;128:577–91. <https://doi.org/10.1111/jnc.12484>.
110. Sebastian Monasor L, Muller SA, Colombo AV, Tanriover G, Konig J, Roth S, et al. Fibrillar Abeta triggers microglial proteome alterations and dysfunction in Alzheimer mouse models. *Elife*. 2020;9:e54083. <https://doi.org/10.7554/eLife.54083>.
111. DeTure MA, Dickson DW. The neuropathological diagnosis of Alzheimer's disease. *Mol Neurodegener*. 2019;14:32. <https://doi.org/10.1186/s13024-019-0333-5>.
112. Malek-Ahmadi M, Perez SE, Chen K, Mufson EJ. Neuritic and diffuse plaque associations with memory in non-cognitively impaired elderly. *J Alzheimers Dis*. 2016;53:1641–52. <https://doi.org/10.3233/JAD-160365>.

113. Knowles RB, Wyart C, Buldyrev SV, Cruz L, Urbanc B, Hasselmo ME, et al. Plaque-induced neurite abnormalities: implications for disruption of neural networks in Alzheimer's disease. *Proc Natl Acad Sci USA*. 1999;96:5274–9. <https://doi.org/10.1073/pnas.96.9.5274>.
114. Mahley RW, Rall SC Jr. Apolipoprotein E: far more than a lipid transport protein. *Annu Rev Genomics Hum Genet*. 2000;1:507–37. <https://doi.org/10.1146/annurev.genom.1.1.507>.
115. Spangenberg E, Severson PL, Hohsfield LA, Crapser J, Zhang J, Burton EA, et al. Sustained microglial depletion with CSF1R inhibitor impairs parenchymal plaque development in an Alzheimer's disease model. *Nat Commun*. 2019;10:3758. <https://doi.org/10.1038/s41467-019-11674-z>.
116. Bennett RE, Bryant A, Hu M, Robbins AB, Hopp SC, Hyman BT. Partial reduction of microglia does not affect tau pathology in aged mice. *J Neuroinflammation*. 2018;15:311 <https://doi.org/10.1186/s12974-018-1348-5>.
117. Kim J, Basak JM, Holtzman DM. The role of apolipoprotein E in Alzheimer's disease. *Neuron*. 2009;63:287–303. <https://doi.org/10.1016/j.neuron.2009.06.026>.
118. Gratuze M, Jiang H, Wang C, Xiong M, Bao X, Holtzman DM. APOE antibody inhibits abeta-associated tau seeding and spreading in a mouse model. *Ann Neurol*. 2022;91:847–52. <https://doi.org/10.1002/ana.26351>.
119. Xiong M, Jiang H, Serrano JR, Gonzales ER, Wang C, Gratuze M, et al. APOE immunotherapy reduces cerebral amyloid angiopathy and amyloid plaques while improving cerebrovascular function. *Sci Transl Med*. 2021;13:eabd7522. <https://doi.org/10.1126/scitranslmed.abd7522>.
120. Liao F, Li A, Xiong M, Bien-Ly N, Jiang H, Zhang Y, et al. Targeting of non-lipidated, aggregated apoE with antibodies inhibits amyloid accumulation. *J Clin Invest*. 2018;128:2144–55. <https://doi.org/10.1172/JCI96429>.
121. Jucker M, Walker LC. Self-propagation of pathogenic protein aggregates in neurodegenerative diseases. *Nature*. 2013;501:45–51. <https://doi.org/10.1038/nature12481>.

ACKNOWLEDGEMENTS

TV received funding from the Research Council of KU Leuven, the Queen Elisabeth Medical Foundation for Neurosciences and the VIB. IDW received funding from Stichting Alzheimer Onderzoek Belgium (Standard Grants – Grant Cycles started 2021–2024, SAO2020022, SAO20240028) and from Methusalem Fund UHasselt. Scholarships of FWO supported ICS (postdoc) and JH (PhD) (G0C6819N, 1190025N). SK is a PhD assistant supported by Hasselt University. BB received funding from the Special Research Foundation of UHasselt (BOF17DOCLI01). MK was supported by a SALK-grant from the government of Flanders, by an Odysseus-grant (G0G1216FWO) and senior research project (G080121N) of the FWO and by a BOF grant (21GP17BOF) from Hasselt University.

AUTHOR CONTRIBUTIONS

SV, AJ, MGdR, BJ, CL, ICS acquired the majority of experimental data, specific aspects were acquired by CL, PBL, ICS, SK, JH, EV, YW. SV, AJ, MGdR, BJ performed data

analysis. SV, AJ, MGdR, BJ, CL, PBL, JH, YW, EV performed animal care and experiments. YAA, TV, MK, AS, MGdR, SP, SK, BB, SV, CL, ID were involved in the scRNA seq experiment execution, data analysis and interpretation. SV, AJ, MGdR, BJ, and ID, conceptualized the study, prepared the manuscript and the figures. SV, AJ, MGdR, BJ, YAA and ID wrote the manuscript. All authors revised and approved the manuscript. Funding was provided by the different research teams MK, TV, BB, YAA, ID.

COMPETING INTERESTS

The authors declare no competing interests.

ETHICS APPROVAL AND CONSENT TO PARTICIPATE

The ethical committee for animal welfare of Hasselt University approved all the performed experiments. All methods were performed in accordance with the relevant guidelines and regulations.

ADDITIONAL INFORMATION

Supplementary information The online version contains supplementary material available at <https://doi.org/10.1038/s41380-025-03036-7>.

Correspondence and requests for materials should be addressed to Ilse Dewachter.

Reprints and permission information is available at <http://www.nature.com/reprints>

Publisher's note Springer Nature remains neutral with regard to jurisdictional claims in published maps and institutional affiliations.



Open Access This article is licensed under a Creative Commons Attribution-NonCommercial-NoDerivatives 4.0 International License, which permits any non-commercial use, sharing, distribution and reproduction in any medium or format, as long as you give appropriate credit to the original author(s) and the source, provide a link to the Creative Commons licence, and indicate if you modified the licensed material. You do not have permission under this licence to share adapted material derived from this article or parts of it. The images or other third party material in this article are included in the article's Creative Commons licence, unless indicated otherwise in a credit line to the material. If material is not included in the article's Creative Commons licence and your intended use is not permitted by statutory regulation or exceeds the permitted use, you will need to obtain permission directly from the copyright holder. To view a copy of this licence, visit <http://creativecommons.org/licenses/by-nc-nd/4.0/>.

© The Author(s) 2025